–Tutor/s

Dra. Maria Guix Noguera
Department of Material Science and Physical Chemistry

Dr. Josep Puigmartí-Luis
Department of Material Science and Physical Chemistry

Grau en Enginyeria Química

UNIVERSITAT DE BARCELONA

Final Degree Project

Spatially controlled chaotic mixing in microfluidic devices using local geometrical features to enhance reactivity conditions

John Patrick Palma Lomboy

June 2025

Somewhere, something incredible is waiting to be known.

Carl Sagan

En primer lloc, voldria expressar el meu profund agraïment als neus tutors, la Dra. Maria Guix Noguera i el Dr. Josep Puigmartí-Luis, per la seva orientació, dedicació i suport al llarg de tot el desenvolupament d'aquest projecte. En especial, a João Vale, per la seva constant guia, disponibilitat i implicació, que han estat fonamentals durant tot el procés. Ha estat un plaer formar part del grup de recerca ChemInFlow.

D'altra banda, vull agrair a la meva família, amics i parella pel seu suport incondicional i per ser sempre al meu costat durant aquesta etapa.

CONTENTS

SUMMARY I

RESUM III

SUSTAINABLE DEVELOPMENT GOALS V

1. INTRODUCTION 1
1.1.Microfluidic systems 1
1.1.1.Development of microfluidic systems 2
1.1.2.Current applications 3
1.1.3.Microreaction Technology (MRT) 3
1.2.Flow regime 4
1.2.1.Governing equations 5
1.2.2.Mass transport 6
1.2.3.Stokes and Peclet number 7
1.3.Chaotic mixing 8
1.4.Computational Fluid Dynamics (CFD) Simulations 9
1.4.1. Importance of the quality of the mesh 9
1.4.2. Mesh Topologies in CFD 10
1.4.2.1. Structured vs Unstructured Meshes 10
1.4.2.2. Polyhedral Meshes 11

2. OBJECTIVES 13

3. SIMULATIONS OF THE LOC DEVICES 15
3.1. Geometry and boundary conditions 16
3.2. Mesh configuration 17
3.3. Simulation configuration 18
3.3.1. Simulation Parameters 18
3.3.2. Pathline display 20
3.3.3. Pathline animation 20

4. EXPERIMENTAL SECTION 21
4.1. Materials and methods 21
4.2. Microchip fabrication 21

4.2.1. Master mold printing 22
4.2.2. PDMS chip replication protocol 22
4.2.3. LoC final configuration 23
4.3. Sample preparation 23
4.3.1. Fluorescent magnetic particles used as tracers 24
4.3.2. Dye color mixing test 24
4.3.3. Electrochemical validation 24
4.4. Device Operation 26
4.5. Data Acquisition 27
4.6. Image Processing 28

5. RESULTS AND DISCUSSION 29
5.1. Evaluation of the Non-Dimensional Numbers 29
5.1.1. Reynolds Number (Re) 29
5.1.2. Stokes number (Stk) 30
5.1.3. Peclet Number (Pe) 31
5.2. CFD Simulation Results of the Microfluidic devices 32
5.3. Optimization of the LoC Devices 34
5.4. Experimental results 35
5.3.1. Microparticles used as tracers 35
5.3.2. Dye color mixing test 35
5.3.3. Electrochemical validation 36

6. CONCLUSIONS 38

7. FUTURE WORKS 40

REFERENCES AND NOTES 41

ACRONYMS AND SYMBOLS 45

APPENDICES 47

APPENDIX 1: DIMENSIONS OF THE MICROFLUIDIC DEVICES 49

APPENDIX 2: PATHLINE DISPLAY OF THE CFD SIMULATIONS 55

APPENDIX 3: EXPERIMENTAL VIDEOS 57

SUMMARY

Lab-on-a-chip technology has enabled chemical reactions to take place under precisely controlled flow conditions, improving reproducibility and efficiency. However, microscale mixing remains a challenge due to the predominantly laminar flow regime, which lacks turbulent eddies that are typically used to enhance mass transport at larger scales

In some specific cases, enhanced micromixing is desired to increase mass-transport in certain areas of the chip. Such an effect could be achieved by using pumps, but more advanced configurations have been explored to indirectly induce mixing in well-defined areas of the microchannel.

For example, chaotic mixing has been implemented to enhance mixing in low Reynolds number flows. This method leverages base-relief structures on the microchannel surface, inducing flow perturbation while improving mixing efficiency. Unlike active methods such as pumps, chaotic mixing allows for localized and controlled mixing in the microfluidic device through geometrically optimized channel designs.

This final degree project focuses on the rational design and implementation of chaotic advection in microchannels, integrating computational simulations and experimental validation. To evaluate the impact of the different geometries on the mass-transport undergoing events, two different case studies are performed in lab-on-a-chip devices fabricated applying microfabrication techniques where printed mold is used. The first study will rely on the use of micrometric (i) passive particles and (ii) colored dyes to track such flows, while the second one will be based on the electrochemical detection of Prussian blue in a lab-on-a-chip system with integrated miniaturized sensors where performance in real sensing applications of our optimized device will be evaluated.

Different areas of expertise will be covered, from fluid dynamics to microfabrication technologies, performing a systematic study to find out how materials and design are key to

developing advanced microfluidic systems, optimizing their design for enhanced performance in chemical and biosensing applications.

Keywords: Lab-on-a-chip, microfluidic devices, chaotic mixing, mass transport, fluid dynamics, computational simulations, microfabrication, 3D printing.

RESUM

La tecnologia lab-on-a-chip ha permès realitzar reaccions en condicions controlades, amb una reproductibilitat i eficiència destacable gràcies a l'ús de volums de reactius molt petits i sistemes de control molt avançats respecte les pressions aplicades. En microcanals de l'odre de micròmetres, generalment s'obtenen fluxos laminars que poden ser de gran interès per obtenir materials amb estructures cristal·lines i propietats molt ben definides. Tot i així, en alguns casos concrets, és necessari precisament obtenir fluxos turbulents per tal d'obtenir una mescla activa en seccions localitzades del microcanals on, per exemple, es porti a terme un procés de sensat on es requereixi d'un augment de transport de massa local. Aquest efecte es podria aconseguir mitjançant bombes, però s'han explorat configuracions més avançades per induir indirectament aquesta mescla en àrees ben definides del microcanal.

Una d'aquestes tècniques és la mescla caòtica, un mètode passiu microfluídic dissenyat per millorar la mescla en règims de baix nombre de Reynolds. Aquesta estratègia utilitza estructures amb relleus a la base del microcanal, les quals pertorben el flux i n'augmenten l'eficiència de mescla. A més, aquestes estructures són fàcils de fabricar, cosa que fa que la mescla caòtica sigui una solució pràctica i escalable per a aplicacions microfluídiques.

El treball de recerca està distribuïda en diferents parts, centrant-se inicialment en el disseny i simulació de les diferents geometries que s'han estudiat i com aquests afecten a la mescla dins del canal. Cal destacar, que aquestes geometries no només s'integren en la superfície del microcanal, sinó que també s'ha fet un estudi en com integrar-les a l'inferior del canal creant així cambres de mescla caòtica. La raó per la qual s'han explorat aquests dissenys, és que l'ús de tècniques en impressió 3D disponibles al grup permet portar-los a terme de manera experimental.

Durant el TFG, s'han dut a terme no només les simulacions teòriques i el treball experimental, sinó que també el tractament de dades corresponent relatiu a les dades obtingudes amb els diferents sistemes de control, incloent el monitoratge de les partícules passives, mescla amb colors i validació numèrica mitjançant un experiment amb sensors electroquímics.

Paraules clau: Lab-on-a-chip, microfluids, mescla caòtica, disseny de microcanals, microfabricació, transport de massa, impressió 3D.

SUSTAINABLE DEVELOPMENT GOALS

The SDGs provide a structured roadmap to address global socio-economic and environmental challenges. Green and sustainable chemistry are integral to advancing these goals, particularly under the 2030 Agenda, which outlines 17 key objectives for sustainable development.

This project is closely linked to SDG 9 (Industry, Innovation and Infrastructure) by advancing microfluidic technologies that promote sustainable laboratory innovation. Through the integration of CFD simulations, model design and precision microfabrication, it enables scalable, efficient and controllable lab-on-a-chip systems enhancing localized chaotic mixing for chemical, biomedical and environmental applications.

By advancing microfluidic design and optimization, this work contributes to SDG3 (Good Health and Well-Being) through enabling precise control over fluid behavior, which is critical in diagnostic tools and point-of-care testing. Improved mixing in microfluidic devices enhances the performance of assays used in disease detection and monitoring.

1. INTRODUCTION

The phenomena governing fluid flow are different depending on the scale range. For example, gravity forces have little influence in micro-flows because the height of the fluidic devices is very small, (typically < 1 mm) [1]. Another striking difference is the absence of turbulent flow in small-scale fluids. Instead, microfluidic flows are predominantly characterized by low Reynolds number regimes, where viscous forces dominate over inertial forces, resulting in a predictable laminar flow behavior. Additionally, molecular diffusion, typically negligible for mass transport in macroscale systems, becomes a dominant mechanism at this scale [2]. Therefore, microfluidic devices can be interesting platforms for performing chemical reactions in specific reaction-diffusion conditions that may not be attainable in macroscale systems.

1.1. MICROFLUIDIC SYSTEMS

Microfluidics is a field where science and technology are performed in channels ranging from micrometers to millimeters scales, combining principles of fluid dynamics, materials science and engineering to develop highly efficient miniaturized systems for chemical and biological applications. This miniaturization of analytical testing and laboratory processes are often referred to as lab-on-a-chip (LoC), biochip or micro-total analysis system (μTAS) [3].

LoC or μTAS devices allow chemical and biological reactions to be performed in a controlled microfluidic system. This technology enhances reproducibility and efficiency by using smaller amounts of fluid while minimizing reactant consumption [4]. The high surface-volume ratio and improved control over mass and heat transfer enables precise control of microscale processes [5], ensuring rapid and reliable analytical processes while minimizing costs, reducing environmental impact and mitigating contamination risks [3].

Having this high-precision analysis and enhanced sensibility at the micro-scale, microfluidic systems have gained prominence on the scene over the past two decades for chemistry, biology, medicine or engineering applications among others [5].

1.1.1. Development of microfluidic systems

In the initial stages of microfluidic device fabrication, silicon and glass served as the primary substrates. Silicon presents a high elastic modulus (230-180 GPa), making it difficult to fabricate active fluidic components such as valves and pumps. Although it is transparent to infrared radiation, its opacity to visible light makes typical fluorescence detection or fluid imaging challenging for integrated structures. This issue is easily overcome by using transparent substrates such as polymers or glass [6].

Glass is compatible with biological samples, has relatively low nonspecific adsorption and is not gas permeable. However, due to its composition-dependent elastic modulus, hybrid devices are required for active components such as valves and pumps, just as in the case of silicon [6]. Even though microfluidic devices can be successfully fabricated using this material, the micro-patterning process on glass is so time-consuming, fabrication methods are slow, and the high material costs make them impractical for disposable applications [7] [8].

Polymers are organic-based, long-chain materials that have gained significant traction in microfluidics in the past 15 years [6] and they are a very attractive cost-effective and less fragile alternative to glass and silicon [7]. Among them, polydimethylsiloxane (PDMS) is one of the most widely used materials for microfluidic device fabrication in research laboratories [3]. PDMS is a highly flexible material with a low elastic modulus (300-500 kPa) [6], making it an ideal substrate enable to incorporate very useful microfluidic components, such as pneumatic valves and pumps [4]. Additionally, its optical transparency down to 230 nm enables compatibility with various optical detection methods and it is also compatible with biological studies due to its impermeability to water, nontoxicity to cells and permeability to gases. A final major advantage of PDMS over glass and silicon is the ease of fabrication and bonding to other surfaces, facilitating rapid prototyping and integrating in microfluidic applications [9].

1.1.2. Current applications

As mentioned before, LoC devices have provided major advances in different scientific fields such as pharmacy, bioengineering, chemistry, materials and chemical engineering among others. LoC devices are widely used for rapid diagnostics of diseases such as COVID-19, HIV, malaria or cardiovascular markers, where immunoassays or polymerase chain reaction (PCR) are integrated into miniaturized microfluidic formats. These are bioanalytical techniques for measuring the presence and concentration of antigen in biological liquid [3] used for clinical, pharmaceutical and scientific research laboratories for diagnostics [4]. In parallel, LoC has also been employed in environmental monitoring applications, such as the assessment of water quality [10] through the detection of contaminants like pollutants, heavy metals, nitrates, and microbial contaminants. Additionally, LoC devices with miniaturized biosensing elements have demonstrated a real-time detection capability for aerosolized pathogens, including bacteria and viruses [11] [12].

1.1.3. Microreaction Technology (MRT)

Taking advantage of the precise control that microfluidic systems provide, the development of industrial-scale mixing technologies at the microscale has emerged as a pivotal advancement in industrial processing, particularly within the framework of process intensification [13]. Although turbulence enhances mixing, it introduces flow irregularities and gradients in temperature and concentration. Microreaction Technology (MRT) provides a scalable platform, enabling an enhanced mass and heat transfer, reactant mixing [14] and a precise control over reaction kinetics. These advantages contribute to increased process safety and efficiency in continuous-flow chemical systems [15].

Due to the high operational temperatures and pressures, MRT devices are fabricated using hard substrates, including silicon, glass, ceramics or metallic alloys. Due to the demand of high throughput platforms where the susceptibility to clogging is reduced, MRT systems are fabricated with larger microchannels than microfluidics devices, scaling up RT platforms to the millimeter range [13], enabling a more controlled and predictable fluid dynamics.

Working with this technology, efficiency is increased, and plant sizes can be scaled down reaching volumes of industrial interest [13]. There is growing interest in the chemistry community in transitioning from the classical flask procedures towards automated systems using artificial intelligence, optimizing nearly in real-time synthesis of certain reactants [16]. Further acceleration in development of multistep synthesis could be realized by integrating synthesis planning and automated synthesis [17], putting MRT an estimation place global market valuation of MRT at approximately USD 1 billion [13].

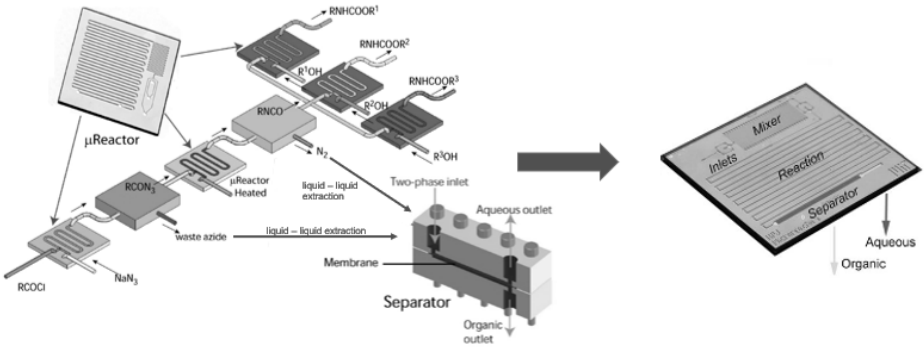

Figure 1. Display of a microreactor and its configuration. Image adapted from [34].

1.2. FLOW REGIME

Understanding how fluids perform in a microscale requires an understanding of parameters including fluid velocity, flow rate, pressure gradient, diffusion coefficient and chemical interactions within the micro-channels [18].

Flow in microfluidic systems encounter resistance by diffusive forces due to pressure gradients, gravity effects and viscous interactions [19]. For liquids, the viscosity of the fluid is the main force that causes this resistance, which in turn is determined by the ratio of the shear stress (σ) to the shear rate (γ) [2][3].

$$\sigma = \frac{F}{A} \qquad (1)$$

$$\gamma = \frac{dv}{dl} \qquad (2)$$

Where in σ, F, is the force acting on the area A and in γ, $\frac{dv}{dl}$ is the velocity gradient.

By combining equations (1) and (2), the mathematical expression of viscosity (μ) is:

$$\mu = \frac{\sigma}{\gamma} \qquad (3)$$

Due to small-scale geometry of microfluidic devices, fluid flow within microchannels remains in a laminar regime, where mixing is predominantly governed by molecular diffusion rather than convective turbulence [18]. For this laminar regime to occur, the Reynolds number (Re) is a dimensionless parameter that quantifies the ratio of inertial viscous forces must be lower than ≈ 1000 [20]:

$$Re = \frac{\rho \cdot v \cdot d}{\mu} \qquad (4)$$

Where ρ is the density, d is the diameter – it can be also written as w for squared-sectioned channels representing the corresponding width –, and v is the average fluid velocity in the channel.

For stationary regimes ($\frac{\partial v}{\partial t} = 0$), inertia and viscous forces appearing in (4) can be estimated. Therefore, the Reynolds number can be written as [13]:

$$Re = \frac{Inertial\ forces}{Viscous\ forces} \qquad (5)$$

In microfluidic systems, Re typically approaches a range of values between 10^{-1} to 1 due to the small-length devices used for analytical performances. In such systems, fluid velocities do not exceed 1 cm/s and transverse channel dimensions are on the order of 100 μm. This indicates that viscous forces overwhelmingly dominate over inertial forces in the microscale [13], leading to the generation of interesting and easily controlled mass transport regimes.

1.2.1. Governing equations

In microfluidic systems, precise control overflow parameters and fluid rheological properties are essential, as well as understanding the undergoing chemical reactions in detail [21]. Navier-Stokes equations are a set of partial differential equations that describe the motion of viscous fluids. For an incompressible fluid with constant density and viscosity, and negligible gravity – typical assumptions in microfluidic applications –, the corresponding Navier-Stokes equation is [19]:

$$\frac{\partial(\rho\vec{v})}{\partial t} + \rho\vec{v} \cdot \nabla\vec{v} = -\nabla P + \mu\nabla^2\vec{v} \qquad (6)$$

Where t is the time, $\vec{v}$ is the fluid velocity, ρ is the density, P the pressure and μ is the viscosity. The left side of the equation represents the material momentum caused by the convective acceleration of the fluid, while the right side characterizes the forces present in the system, such as external forces, pressure gradients and viscosity changes [19]. The relationship between these forces and accelerations allows to formulate a diverse set of parameters that define the resulting fluid motion, heat, and mass transport among other phenomenon taking place in the system.

Mass conservation, also known as the continuity equation, is a fundamental principle in fluid dynamics, stating that mass cannot be created or destroyed in a closed system [20] [21]. In general terms, the continuity equation is described as [19]:

$$\frac{\partial\rho}{\partial t} + \nabla \cdot (\rho\vec{v}) = 0 \qquad (7)$$

Following the assumptions to describe the Navier-Stokes equation, where density is constant, equation (7) simplifies into [19]:

$$\nabla \cdot \vec{v} = 0 \qquad (8)$$

This implies that the divergence of the velocity field must be zero, ensuring that the net volumetric flow into any point in the domain is equal to the net flow out [21]. It is a constraint imposed on the velocity field that must be satisfied at every point in the computational domain [19] [20].

1.2.2. Mass transport

Diffusion: diffusion is the transport mechanism that describes the molecule's movement as a drift from one region to another, resulting in a net flux of mass in response to spatial concentration gradients. In order to describe and understand this transport mechanism, Fick's law is used. Fick's law postulates that the solute will move from a region of high concentration to a region of low concentration across a concentration gradient [2]:

$$\frac{\partial C}{\partial t} = D\nabla^2 C \qquad (9)$$

Where D is the diffusion coefficient and ∇C is the concentration gradient.

Advection (Convection): Advection is the transport mechanism of molecules governed by the velocity field of the fluid due to bulk motion in a particular direction. Convection is the combination of both advection and diffusion at the same time. Advection can be further classified into *free advection*, where no external forces intervene on the fluid's motion and *forced advection* is where the fluid is induced by external driving forces [2] [19].

Most of the systems are not governed by one single state but in a combination. Even in the case of advection, where the fluid velocity is nonzero, we get the following convection-diffusion equation [2]:

$$\frac{\partial C}{\partial t} + v \cdot \nabla C = D\nabla^2 C \qquad (10)$$

1.2.3. Stokes and Peclet number

Stokes (Stk) and Peclet (Pe) numbers are great dimensionless numbers that characterize the behavior and tendencies of the fluid and the particles in suspension along a microchannel [20]. These non-dimensional numbers will serve as a criterion to decide which size of particles to use to evaluate the generated fluid flows in Loc devices.

Stokes number: characterizes the behavior of particles suspended in a fluid flow, specifically on how well a particle can undergo changes through the fluid's motion [20]. In microfluidic systems, – for a low Re number and spherical particles – the Stokes number is written as:

$$Stk = \frac{\rho_p d_p^2 v}{18\mu L} \qquad (11)$$

Where ρ_p is the particle density, d_p^2 is the particle diameter and L is the length.

- For $Stk \ll 1$: the particle has a low inertia and follows the fluid streamlines, meaning that the particle will be responsive to changes in the flow. This type of behavior is characteristic from small particles.

- For Stk ≫ 1: the particle has a high inertia and tends to maintain its initial motion, not adapting quickly to fluid velocity changes, meaning that in some point the particles will deviate from the flow path.
- For Stk ≈ 1: Indicates a dynamic equilibrium where both particle inertia and fluid forces significantly determine the pathline flow, resulting in trajectories that are sensitive to changes in both.

Peclet number: Quantifies the relative importance of advective (bulk transport) over diffusion (molecular transport) of a physical quantity such as heat or mass. For mass transfer, Peclet number is described as [2] [20]:

$$Pe = \frac{vL}{D} \qquad (12)$$

- For Pe ≪ 1: mass transport is governed by diffusive flux. Under such conditions, convective contributions are negligible, and the scalar field evolves gradually under concentration gradients, leading to homogenization of the species within the domain.
- For Pe ≫ 1: advective transport dominates over molecular diffusion, resulting in solute move along the flow direction, with minimal transverse mixing due to the relatively slow diffusive flux.

1.3. CHAOTIC MIXING

As mentioned in previous sections, microfluidic systems work in low Re numbers, where laminar flows govern the fluid flow and turbulence is negligible. Though turbulence enhances mixing, it induces unpredictable flows and on reacting mixing, producing potential undesired components. Strook et al. (2002) [22], introduces chaotic mixing as a potential mixing technique in this micrometric scale where, due to absence of turbulent flows, molecular diffusion along the microchannels is slow. This technique consists in modifying conventional and simple microfluidic channels – squared-section channels – by changing its geometry or adding eddies and obstacles along the surface. With this approach, the fluid flow presents a chaos on its streamlines along the microchannel enhancing mass transport via diffusion at low Re numbers. In Strook et al. (2002) [22], the design presented eddies at the bends in the channel, inducing chaotic stirring at low Re

numbers (0 < Re <100), having different experimental results by changing boundary conditions like the height of the channel, the depth of the ridges and the flow rate used, among others.

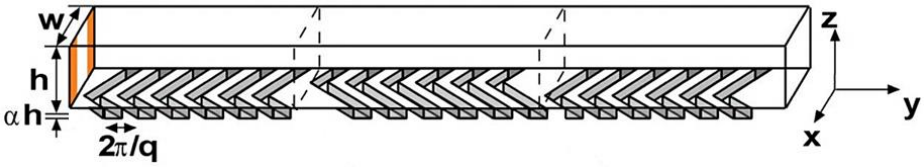

Figure 2. Design referred as Staggered Herringbone mixer (SHM) used for the experiments performed in Stroock et al. (2002) [22]. Image adapted from [22].

1.4. COMPUTATIONAL FLUID DYNAMICS (CFD) SIMULATIONS

Computational fluid dynamics (CFD) represents a fundamental aspect in the future of engineering, enabling the digital modelling and analysis of transport processes involving fluid flow and scalar transport like mass, heat, and concentration transfer [23]. These transport processes are described by mathematical models explained in section 1.2.1, which are solved through different numerical methods enabling a rapid and accurate results [24].

These CFD codes can create virtual prototypes of complex domain across a wide range of scales, from industrial macroscale processes – such as internal areas of distillation columns, a baffled reactor, etc. – to a microscale environment [24]. These domains are discretized into small cells or nodes (control volumes) which the Navier-Stokes and associated conservation equations are numerically solved [25] [26]. In this project the software used to perform the simulations was ANSYS Workbench 2024 R2, a commercial and academical CFD package that uses finite volume method to solve and discretize the governing equations, using a coupled solver algorithm to enhance convergence and stability [26].

1.4.1. Importance of the quality of the mesh

In CFD simulations, meshing is a key stage where the geometry is divided into small computational elements for numerical resolution of the governing equations [24]. The quality of the mesh generated will directly affect on the accuracy, numerical stability, computational efficiency and overall validity of the results of the simulations [2] [23].

A precise mesh construction ensures a proper representation of pressure, velocity or temperature gradients facilitating the capture of complex phenomena, such as recirculation zones or pressure drops, while preventing critical geometric features [27] [25].

As mentioned before, the mesh quality critically influences numerical stability and robustness of CFD solvers [23]. Elements that present high skewness, non-orthogonality, or poor aspect ratios can negatively impact solution precision and hinder residual convergence, potentially leading to divergence or non-physical results. On the other hand, an excessively dense mesh can increase computation time without improving results [28].

1.4.2. Mesh Topologies in CFD

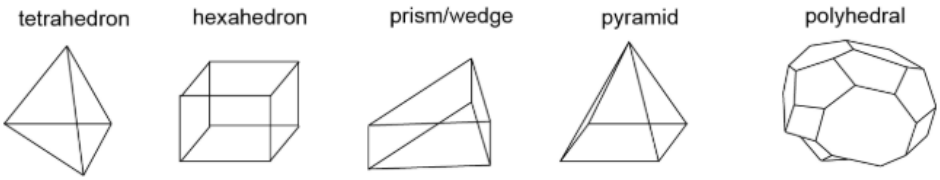

Figure 3. Different type of mesh elements. Image adapted from [24].

1.4.2.1. Structured vs Unstructured Meshes

Structured meshes consist of regularly arranged elements – typically quadrilaterals in 2D and hexahedra in 3D – organized in a grid-like topology [25]. The connectivity between nodes is determined through indexing, which allows an efficient usage of memory storage optimized computational performance. Due to their inherent organization, these meshes are known for their numerical diffusion, fast convergence rates and high accuracy in aligned flows. [23].

However, their application is limited to domains with complex or curved geometries, where generating a structured grid can become impractical and local refinement is also difficult, as it often requires significant adjustments to the global mesh structure [23] [28].

Unstructured meshes are composed of elements with non-uniform topology, such as triangles (2D) and tetrahedra (3D), making them highly adaptable to complex geometries. Their compatibility with automated meshing algorithms has established this type of meshes as a standard in industrial CFD applications [25] [28].

Despite their geometric adaptability, unstructured meshes typically require a significantly larger number of elements than structured meshes to achieve similar levels of accuracy. Poor element quality – such as high skewness or non-orthogonal alignment – can affect convergence and introduce computational errors [25].

1.4.2.2. Polyhedral Meshes

Polyhedral meshes present a highly effective solution by combining the geometric flexibility of unstructured grids with significantly improved convergence characteristics and stability [28]. A typical polyhedral element – featuring 12 to 14 faces – effectively replaces several tetrahedral elements, reducing mesh density while preserving accuracy (see in Figure 4). This reduction in cell number directly contributes to shorter computation times and more efficient simulations, as fewer elements need to be solved [27] [25]. Their inherently isotropic configuration facilitates lower discretization errors, better gradient approximation from adjacent cells and improved solver stability and convergence. These advantages collectively yield a mor computationally efficient simulation process [28].

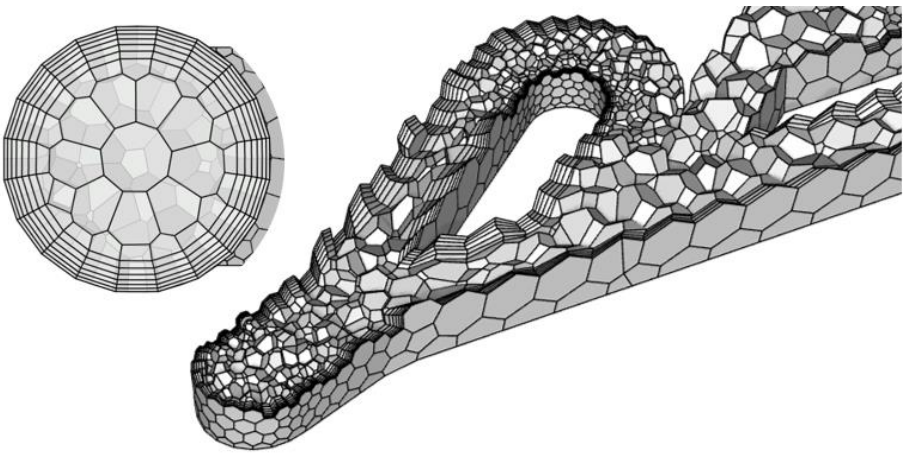

Figure 4. Cross-sectional view of the Tesla Valve model, highlighting the internal polyhedral structure; top-view visualization of the inlet included. Image generated with Ansys Workbench 2024 R2.

2. OBJECTIVES

The main objectives of this project are the design and optimization of a microfluidic device with localized passive mixing at microscale, where laminar regimes govern, to improve bioanalytical and synthesis applications. This project aims to explore and find a methodology that optimizes time and resources to improving the sustainability of certain fabrication or analytical processes, resulting in more reliable and precise results. To accomplish this, the following objectives were addressed:

- Design and evaluate through CFD simulations different microfluidic platforms with distinctive features to induce chaotic streamlines, ideally obtaining localized enhanced mixing.
- Fabricate LoC devices with the designs studied in the CFD simulations and optimize the experimental conditions to evaluate their performance.
- Experimentally test the results obtained from the CFD simulations working at different flow rates tracers/dyes and validate its efficiency by implementing the best design for localized enhanced mixing in an electrochemical setup.

3. SIMULATIONS OF THE LOC DEVICES

The simulation of microfluidic devices is a relatively a rapid process that allows prompt data generation, which is really useful for the LoC designs that will be further fabricated. In fact, if the results obtained for a specific design deviate from the expected ones, the time invested to fabricate, produce and test may extend to 4 days.

In order to optimize time and change the workflow of blindly producing LoC devices without having insight into their later performances, CFD simulations of microfluidic channels served as a valuable predictive tool, enabling data-driven design optimization, experimental iterations and minimizing resource expenditure.

The software used for the CFD simulations was ANSYS Workbench 2024 R2, with the student license provided by the University of Barcelona.

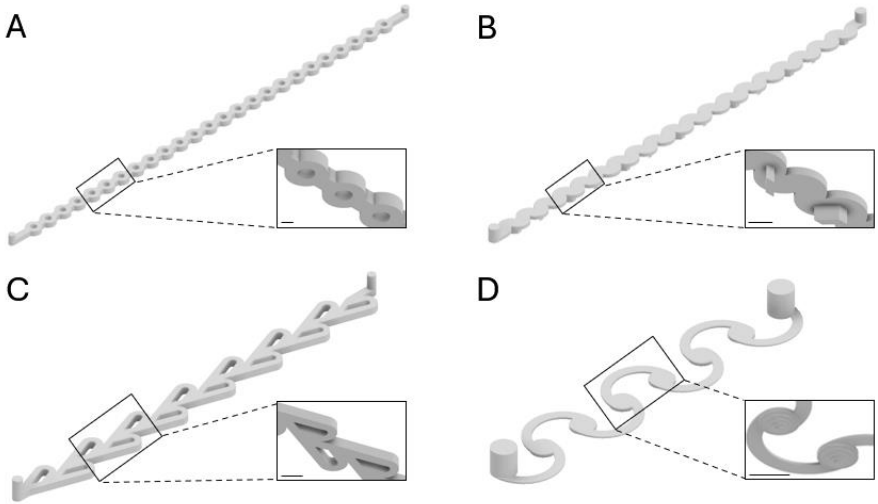

Figure 5. Images of the 3D microfluidic channels designed with Autodesk Inventor with the corresponding bottom view of A) Straight and Rings; B) Curves and Eddies; C) Tesla Valve; D) Vortex Street. Scale bar of all images1 mm.

3.1. GEOMETRY AND BOUNDARY CONDITIONS

The first step for the simulations is to define the geometry of the structure that is going to be simulated. From the Autodesk Inventor software, the same used for the modelling of the master molds for PDMS replica, the body of the 3D is exported as an .stl file for ANSYS to read it.

In this project, the geometry of the microchannels was very complex, characterized by numerous edges and different structures along the channel such as curvature, surface eddies on the surface or sharp edges. To prepare the model for the simulations, 3D structure was preprocessed by selecting some of the options from the Display View control panel to ensure mesh compatibility and geometric integrity –specifically *Simplify Geometry*, *Heal Bodies*, *Replace Missing Geometry* and setting *Clean Bodies* to High–.

Following geometry preparation, the boundary conditions of the structure were defined by selecting the faces which would represent the *Inlet*, *Outlet*, channel *Walls* and the *Fluid* domain (see in Figure 4).

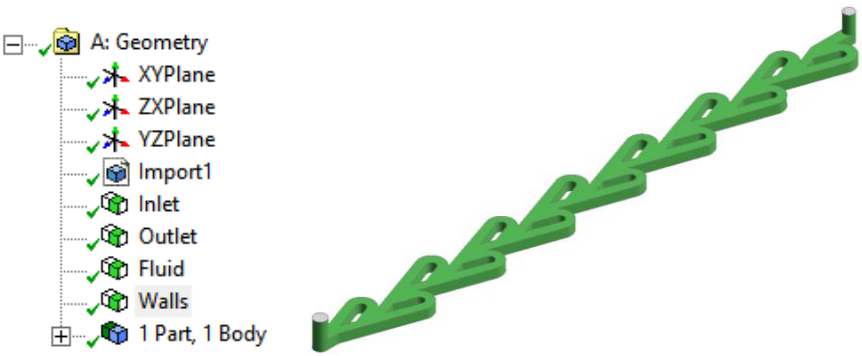

Figure 6. Adapted image from ANSYS Workbench 2024 R2.

3.2. MESH CONFIGURATION

For the CFD simulations performed in this project, the Mesh interface was configured by updating all the parameters displayed in the *Workflow* panel. Under *Describe Geometry* the parameter *The geometry consists of only fluid regions with no voids* was enabled. By selecting this parameter, the solver defined the computational domain as entirely fluid-filled. This step prevents the solver from identifying non-existent solids or discontinuities that would interrupt the numerical convergence.

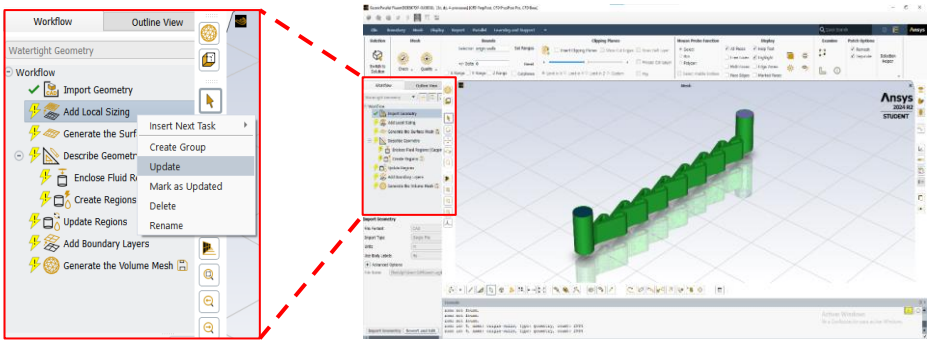

Figure 7. Adapted image from ANSYS Workbench 2024 R2.

Subsequently, in *Add Boundary Layers* the *Offset Method Type* was set to *aspect-ratio* and the *Number of layers* and *First Aspect Ratio* were set to the values of 6 and 12 respectively. Setting these parameters with these values is essential for accurately resolving flow behavior near walls, avoiding the excess generation of small cells and optimizing computational resources while maintaining accuracy. As the last step, in *Generate the Volume Mesh* the *polyhedral* option was selected and generated the final configuration of the mesh for the simulations (see in Figure 6). All the parameters imposed for the mesh generation were the same for all the designs and their respective simulations.

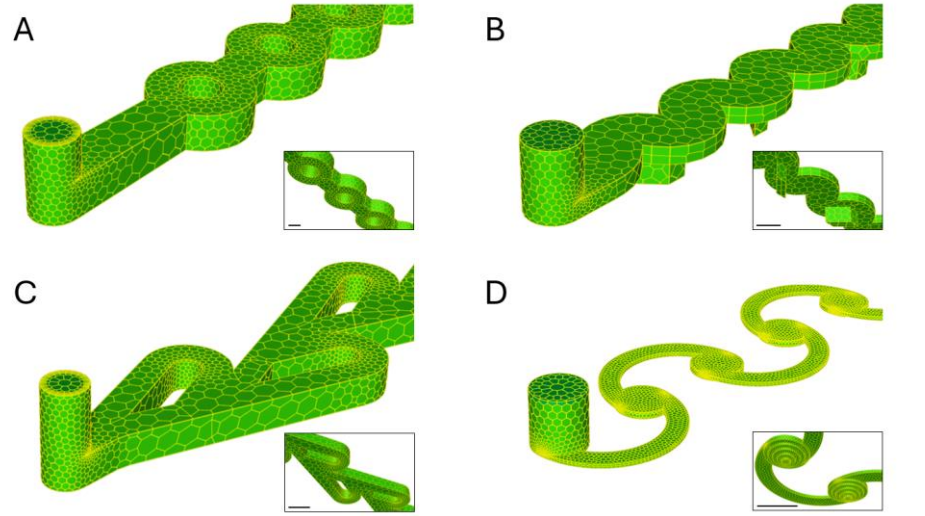

Figure 8. Polyhedral mesh representations of different 3D microfluidic designs and corresponding bottom views. A) Straight and Rings; B) Curves and Eddies; C) Tesla Valve; D) Vortex Street. Scale bar of all images 1 mm. Images generated with Ansys Workbench 2024 R2.

3.3. SIMULATION CONFIGURATION

3.3.1. Simulation Parameters

For the simulation, the setup of the *Viscous Model* chosen was the *Laminar Model*. This model was chosen due to the microfluidic scale and laminar flow domain – Re bellow 2300 – in the microscale, where mixing occurs via diffusion, convection or vortices, not turbulence [22]. This model enables a rapid and stable numerical convergence of the results of our control system rather than the other models presented on the setup – turbulent models – and would yield higher error.

The *Boundary Conditions* panel, is where the different Inlet flow rates are established – 10, 50, 100, 300, 1000 µL/min – used to simulate the fluid performance along the channel in m/s. The values shown in Table 1 are the flow rates used for each model – Tesla Valve (TV), Straight with Rings (SR), Curves and Eddies (CE), Vortex Street (VS) – and its respective conversion to

m/s, which changes depending on the measures of the main channel. For the Outlet, the gauge pressure was 0 Pa, which means that the outlet port is at atmospheric pressure.

Table 1. Flow rates conversion from µL/min to m/s of each design.

	Flow rate (µL/min)				
	10	50	100	300	1000
3D Design	**Flow rate (m/s)**				
TV1	4.938E-04	2.469E-03	4.938E-03	1.481E-02	4.938E-02
TV2	1.228E-04	6.141E-04	1.228E-03	3.685E-03	1.228E-02
SR1	5.556E-04	2.778E-03	5.556E-03	1.667E-02	5.556E-02
SR2	1.852E-04	9.259E-04	1.852E-03	5.556E-03	1.852E-02
CE1	1.905E-03	9.524E-03	1.905E-02	5.714E-02	1.905E-01
CE2	1.905E-03	9.524E-03	1.905E-02	5.714E-02	1.905E-01
CE3	6.667E-04	3.333E-03	6.667E-03	2.000E-02	6.667E-02
CE4	1.667E-04	8.333E-04	1.667E-03	5.000E-03	1.667E-02
VS1	6.233E-03	3.116E-02	6.233E-02	1.870E-01	6.233E-01
VS2	6.233E-03	3.116E-02	6.233E-02	1.870E-01	6.233E-01
VS3	4.363E-03	2.182E-02	4.363E-02	1.309E-01	4.363E-01

The fluid used for the simulations was water. Therefore, the corresponding fluid parameters were added in the *Materials* panel by selecting the component from the *Fluent Database*. Once the fluid was added in the database, a must do step is to select it in *Cell Zone Conditions* as the material of the fluid domain, to ensure that water was the liquid used for the simulations.

To facilitate the convergence of the results in few iterations, the following parameter was set in the *Methods* panel: the scheme selected was *Coupled*. This scheme solves pressure and momentum equations at the same time instead of solving them sequentially.

Before running the simulation, the *Hybrid Initialization* parameters were adjusted, enabling *More Settings* to increase the iteration limit and define a stringent convergence tolerance of $1 \cdot 10^{-6}$, following on literature [28] [29]. This ensured the residuals reached acceptable thresholds, enabling precise resolution of the flow field within the computational domain. Following hybrid initialization, the number of solver iterations was set within the range of 200 to 500, and the computational process was initiated.

3.3.2. Pathline display

To visualize the flow pathlines within the microchannel, it was implemented the *Graphics* > *Pathlines* utility (see in Figure XX). Velocity magnitude was chosen as the color-mapping scalar to visualize variations in flow speed along the streamlines, defining the inlet as the release surface. Subsequently, the mesh was overlaid for spatial referencing by enabling *Draw Mesh* and setting the transparency to 95% to facilitate the visualization of internal flow structures. *Steps* parameter was set to a range of 5000 to 10000 to ensure complete pathline development across the entire channel length.

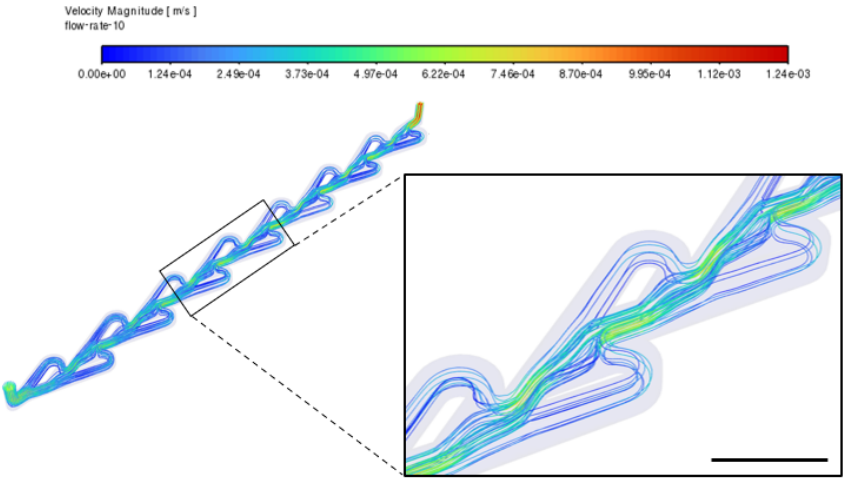

Figure 9. Isometric and closer view of the pathlines generated with TV1 design with a flow rate of 10 µL/min. Image generated ANSYS Workbench 2024 R2. Scale bar of 1 mm.

3.3.3. Pathline animation

Streamline animation was carried out using the CFD-Post module within the Fluent (with Fluent Meshing) results environment. I enabled and configured streamline visualization by setting up the parameters in the *Streamline Settings*: *Domains* > *All Domains*, *Start From* > *inlet*, *Sampling* > *Equally Spaced* and *# of Points* > *5000*. Streamline rendering was specified as *Line Type* with a *Line Width* of 1. In animation module, I selected *Sweep Animation* with *Streamline 1* as the animated object, and playback speed set to *Slow*. To improve visual traceability, symbol display overrides were activated. The animation was subsequently generated and exported in the appropriate directory.

4. EXPERIMENTAL SECTION

4.1. MATERIALS AND METHODS

Resin (Clear Microfluidics Resin V7.0a), Polydimethylsiloxane (PDMS SYLGARD 184 Silicone Elastomer Base), Curing Agent (SYLGARD 184 Silicone Elastomer Curing Agent), Isopropanol, Distilled water, Aluminum Foil, Stirring rod, Cutter, Sealed-edge laundered knitted polyester cleanroom wipers (VWR Spec-Wipe 23x23 cm), Oven (Memmert 30L Oven UF30), CureZone (UV post-curing device), N_2 air (Airon JFP.2), Diaphragm Vacuum Pump (Vacuumbrand MZ 2C), Plasma Cleaner (PDC-002-CE, Harrick Plasma), Manual Hole Puncher (SYNEO Accu-Punch MP 10-UNV), Punch (SYNEO Cutting Edge Diameter 1.65 mm), Ejector Pin (SYNEO SEP-015), 1 mL Plastic Syringe (Fisherbrand 1 mL Syringe), 3 mL Plastic Syringe (Fisherbrand 3 mL Syringe), Syring needles (0.8 x 50 mm, HENKE-JEKT), polytetrafluoroethylene tube (Vici Vour 0.5 mm inner diameter), Syringe Pump (Nemesys CETONI Base 120 and Aladdin AL-1000), Fluorescent Magnetic Particles (UMDG001 COMPEL™ Fluorescent Magnetic COOH, Dragon Green – 3 μm), Blue Dye and Red Dye (Darwin Microfluidic Dyes Bleu Ciel E133 and Rouge Dye E129), MiliQ Water, Iron(III) Nitrate Nonahydrate, Potassium Hexacyanoferrate(III), Potassium Chloride, Potassium Acetate, Acetic Acid Glacial were all purchased from commercial sources. Images were acquired by an inverted microscope (Nikon Eclipse T*i*-U) and Stereoscope (Nikon SMZ-800N), both equipped with a camera (Basler puA1280-54um). The images were processed with Pylon viewer software.

4.2. MICROCHIP FABRICATION

The fabrication of microfluidic devices was based on microfabrication techniques. Initially, a master mold was printed using a high-resolution 3D printer. Afterwards, PDMS was cast, producing a replica of the layout of the channels. Finally, the assembly between the PDMS replica and the glass structure is done by plasma bonding, yielding a sealed microfluidic chip ready to be used for laboratory analysis.

4.2.1. Master mold printing

The technique used for the printing of the master mold is stereolithography (SLA). The printer used is the CADworks Profluidics 285D and provides a high-resolution (dynamic XY resolution of 28.5 μm), ensuring smooth surfaces and precise channel dimensions, allowing the fabrication of master molds of an overall area of 8 cm x 6 cm with diverse microchannel geometries in less than 35 min. The microchannel geometry was designed and optimized using Autodesk Inventor, a CAD 3D software. The printer and the software license were both provided by the University of Barcelona.

After printing the master mold, excess resin was trimmed from the edges of the piece to achieve a well-defined shape, followed by cleaning with isopropanol to remove any residual non-polymerized surface resin and drying it with N_2 air.

For the curing process, the master mold was treated with a high-intensity UV device for 40 min, with the mold being flipped every 10 min ensuring uniform exposure across its surface. As a final curing step, I placed it in an oven at 80 ºC for 48 h. During the first characterization of the microfluidic devices, the master mold was cured in the oven for 24 h. However, when I used the mold for the PDMS replication, the resulting chip presented roughness and imperfections on the structure, indicating that the curing of the mold was incomplete. To address this issue and ensure a complete and uniform curing process, I left the mold in the oven for a longer curing time, being 48h the optimized curing time for molds of 8 cm x 6 cm.

4.2.2. PDMS chip replication protocol

For the mold replication, PDMS and the curing agent were measured in a 10:1 (w/w) ratio and mixed roughly for 2-3 min until a uniform consistency is achieved. The resulting mixture was placed in a vacuum degassing chamber for 15-30 min until all the visible bubbles were removed. A containment bath was assembled by wrapping around some aluminum foil the master mold.

After the degassing of the PDMS mixture, it was poured in the master mold bath and cured in the oven at 80 ºC for 8 h. Once cured, the PDMS was cooled to room temperature and carefully peeled from the mold. The excess of PDMS of the replica was precisely trimmed using a sharp cutter, to obtain the desired shape of the chip. Finally, a manual hole puncher (SYNEO Accu-Punch MP 10-UNV) was used to do the inlets and outlets of the microfluidic device.

4.2.3. LoC final configuration

As the final step, the final configuration of the LoC device was carried out with the already assembled chip. Plasma bonding with oxygen treatment was used to activate both the PDMS layer and the chip surface, in this case a glass slide. This plasma treatment enhances the bonding between the two surfaces by the removing of residual components and replacing PDMS' methyl terminal groups (-CH_3) with silanol groups (-SiOH), which can form covalent bonds (Si-O-Si) leading to an irreversible sealing [30]. Therefore, both the glass and the PDMS chips, with the channel side facing upwards, were placed in the Plasma Cleaner. The chamber was set at 0.6 mmHg by making the vacuum, after which the plasma treatment was performed at a high intensity for 2 min to facilitate surface activation.

To complete the device assembly, the PDMS was manually pressed against the glass substrate, followed by placing it on a heating plate for 2 h at 125 ºC to enhance adhesion and ensure a good assembly of the LoC device.

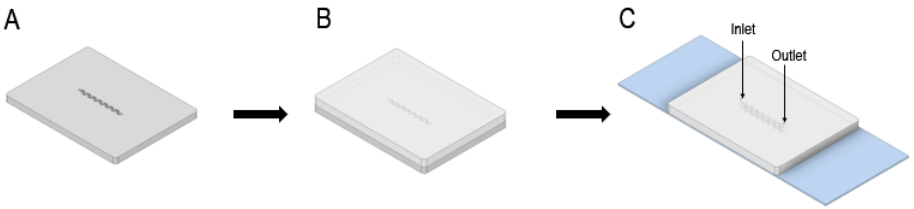

Figure 10. Microchip Fabrication Diagram. A) Master Mold Printing, B) PDMS Replica, C) Final LoC Configuration. Image generated with Autodesk Inventor.

4.3. SAMPLE PREPARATION

To evaluate the flow behavior within the microfluidic channel designs, different experimental observations were done in order to correlate them to the CFD simulations explained in section 3. Two different experimental tests were performed: (i) using magnetic particle solution, and (ii) inserting different dyes in the microfluidic device.

4.3.1. Fluorescent magnetic particles used as tracers

As the passive particles we wanted to use didn't arrive on time for the experiments, alternatively, COMPEL™ Magnetic Microspheres available in the lab were used.

Fluorescent Magnetic particle aqueous solution: to prepare the solution, 3 µL of the COMPEL™ Magnetic Microspheres solution and 0.997 mL of distilled water were added to a 1.5 mL vial. Afterwards this aqueous solution was introduced to a 1 mL syringe.

4.3.2. Dye color mixing test

In order to have an enhanced qualitative visualization of the internal flow dynamics, dye tracing was carried out as a complementary validation method. Given the complexity of the device operation and limited experimental time, only one of the microfluidic designs was implemented into a Y-shaped channel. The design was selected based on its performance presenting potential chaotic streamlines both in CFD simulations and magnetic particles tracking, referring to it as Vortex Street.

Blue dye solution: to prepare a 10% solution, 300 µL of Blue Dye and 2.7 mL of distilled water was added to a 5 mL syringe.

Red dye solution: to prepare a 13.33% solution, 400 µL of Red Dye and 2.6 mL of distilled water was added to a 5 mL syringe.

4.3.3. Electrochemical validation

By integrating chaotic cell units in a LoC chip devices, we do not only achieve controlled mixing that is directly correlated to enhanced mass transport, but also certain secondary flows that have a great impact on the fabrication of chiral materials [31]. In the present TFG, we focused on obtaining a quantitative evaluation of the impact that the chaotic cell units have on the sensitivity of an analytical method. To do so, the design was tested by Irene Vilà i Cibantos (TFG *Integration of miniaturized sensors in lab on a chip devices for enhanced mass transport efficiency*

in Chemistry supervised by Dr. Maria Guix and Dr, Julio Bastos Arrieta). Firstly, a standard electrochemical test was run using a Y-shaped channel as a control experiment, to later test in Vortex Street design.

The model compound that was chosen was Prussian Blue (PB, Iron(III) Hexacyanoferrate(II) or Ferric Ferrocyanide), which presents a characteristic deep blue color and a high chemical stability and ionic conductivity. Prussian Blue is generated by the reaction of Iron(III) Nitrate Nonahydrate ($Fe(NO_3)_3 \cdot 9H_2O$), Potassium Hexacyanoferrate(III) ($K_3[Fe(CN)_6]$), Potassium Hexacyanoferrate(III) ($K_3[Fe(CN)_6]$), Potassium Chloride (KCl), and L-Acid Ascorbic in a buffer solution at pH 5. To study PB generation in a LoC device, we prepared two different solutions that will be injected into each inlet of the microchannel.

Solution A (Sol A): Solution composed by joining all the reagents together. 10 mM $Fe(NO_3)_3 \cdot 9H_2O$, 10 mM $K_3[Fe(CN)_6]$, 0.1 M KCl, Buffer pH 5. Afterwards, the solution was introduced into a 5 mL syringe.

- **Reagent I**: to prepare 100 mL 10 mM, 412,2 mg of Iron(III) Nitrate Nonahydrate were dissolved with MiliQ Water.
- **Reagent II**: to prepare 100 mL 10 mM, 329.3 mg of Potassium Hexacyanoferrate(III) were dissolved with MiliQ Water.
- **Reagent III**: to prepare 100 mL 0.1 M, 745.2 mg of Potassium Chloride were dissolved with MiliQ Water.
- **Buffer**: to prepare 100 mL 10 mM buffer solution at pH 5, 628.3 mg of Potassium Acetate were dissolved with MiliQ Water and then 210 µL of 99.7% Acetic Acid Glacial was added. The pH of the solution was determined with a pHmeter and obtained a value of 4.85.

Solution B (Sol B): to prepare 100 mL 50 mM of L-Ascorbic Acid solution, 880.6 mg of ascorbic acid was dissolved in 100 mL of MiliQ water. This solution had to be kept in the refrigerator to prevent rapid degradation. Afterwards, the solution was introduced into a 5 mL syringe.

The reaction taking place is an in situ redox method, in which Ascorbic Acid acts as a reducing agent to lead to the actual PB generation, taking place between the Hexacyanoferrate(III) and Iron (III) present in solution. The electrochemical tests and the corresponding data treatment

related to the electrochemical validation of the microfluidic device with spatially controlled chaotic mixing were done by Irene Vilà i Cibantos.

4.4. DEVICE OPERATION

Fluorescent Magnetic Particle used as a tracer Test: To prepare the LoC device, the chip was placed in an inverted Nikon T*i*-U microscope. To provide controlled and continuous flow in the chip, the 1 mL syringe was placed in a Nemesys syringe pump (Cetoni), an injection system composed of 5 individual modules, one per each syringe.

The syringe and tubing connection were carefully assembled to avoid air bubbles generation during the experiment. An initial isopropanol injection was performed to enhance the hydrophilicity of the PDMS surface and reduce surface tension along the microchannel and was followed by a water rinse to remove the residual isopropanol, ensuring a fully aqueous environment. To maintain an air-free interface, the syringe pump was set to 300 µL/min until a drop fell, forcing a droplet-to-droplet contact between the syringe and the tubing avoiding bubble generation. Subsequently for the outlet, a vial was connected to facilitate the recovery of the particles and reuse them for the tracking tests of the other designs.

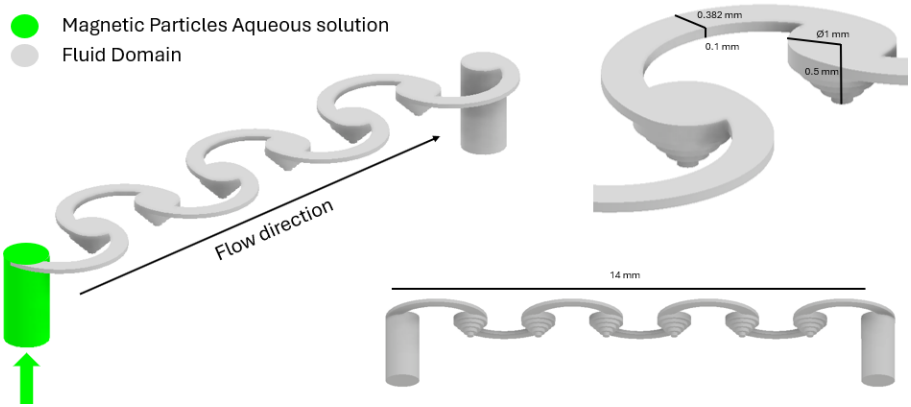

Figure 11. Fluorescent Magnetic Particle as a Tracer test Device Operation and measures of the Vortex Street design. Images generated with Autodesk Inventor.

Dye Color Test and Electrochemical Validation: For both the dye color and electrochemical validation tests, the Vortex Street design was implemented to a Y-shaped channel. The assembly protocol of the LoC device was carried out in a different methodology approach. We used PDMS-to-PDMS reverse clamping mechanism for the closure of the system. The PDMS microchannel layer was cast upside down against a flat PDMS surface in order to have the microchannels on the right position, therefore the inlets and outlets were facing down. It was followed by mounting it on a custom clamping system that applied uniform pressure across both the upper and the lower surfaces, ensuring a tight and uniform pressure along the microfluidic chip and prevent leakage. Afterwards, the microfluidic device was placed on the stereoscope. For this test, to provide a continuous and controlled flow rate, the two syringes that contained both Blue Dye and Red Dye were placed on Aladdin syringe pump with an injection system with two modules that provide the same flow to each of the two syringes, same procedure was followed for Sol A and Sol B for electrochemical validation test. In order to have a fully aqueous interface and free of air bubbles, the same strategy from the magnetic particle tracking test was applied.

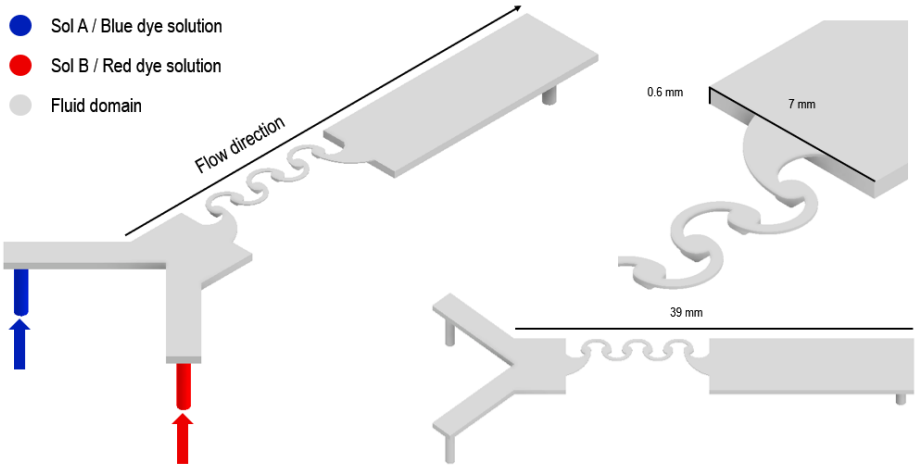

Figure 12. Device Operation of Dye Color and Electrochemical Validation tests and measures of the channel. Image generated with Autodesk Inventor.

4.5. DATA ACQUISITION

For data collection, an inverted Nikon T*i*-U microscope equipped with Basler puA1280-54um Camera was used. The images were taken using Pylon Viewer, an automated image acquisition software used by the group.

For the image collection, we focused on observing only a control node of the microfluidic devices at different flow rates in order to verify the trends obtained from the results of the CFD simulations explained in section 3. This would allow us to verify which designs generate an irregular flow that could lead to chaotic mixing. Therefore, images were taken at a frame rate of 1 frame per 30 milliseconds allowing us to have a very smooth visualization of the videos both at normal and slow motion.

4.6. IMAGE PROCESSING

After the image acquisition, we stored them in TIFF format by organizing them in folders per test. Afterwards, they were processed with Fiji (ImageJ, NIH) to reconstruct the images and obtain the animation of the node control. Same procedure was followed for both streamline tracking tests and dye color tests.

Images from every acquisition were grouped in different folders according to the test performed and the flow rate used for each test. Each folder was loaded in ImageJ to compile them in different videos with a frame rate of 25 fps and 7 fps to obtain a normal speed and slow-motion animation of the tests. The sequences followed were *Image* > *Stacks* > *Images to Stack* and *File* > *Save As* > *AVI* in *JPEG* and selected 25 or 7 fps for each folder.

5. RESULTS AND DISCUSSION

This section presents the results obtained during the development of this project offering a comprehensive interpretation and critical analysis. Emphasis is placed on key aspects to take in account, including optimization of the LoC devices and evaluation of different microfluidic designs, both from theoretical standpoint by performing CFD simulations and the experimental validation of different systems.

5.1. EVALUATION OF THE NON-DIMENSIONAL NUMBERS

The calculation of the non-dimensional numbers enables an early evaluation of the flow regime and the behavior tendency of the particles along the channel. The parameters Re, Stk and Pe are calculated using the Equations (4), (11) and (12) respectively. Regarding the fluid domain, water was the chosen component for both simulations and experimental studies, having a density of ρ = 1000 kg/m^3 and viscosity of μ = 0.001 Pa·s. Also, the dimensions of microfluidic channels used for the numerical resolution are detailed on Appendix 1.

5.1.1. Reynolds Number (Re)

Since all the microchannel cross-sections present square edges, Equation (4) was evaluated under the assumption that the diameter is equal to the width, d=w. As expected, the calculated Reynolds numbers obtained are in the range of 0 < Re < 250, validating that laminar flow is the governing regime (Re below 2300) of our microfluidic systems, and providing us with predictable and controlled flow along the microchannel.

In contrast, the results indicate that by increasing the microchannel width, a higher Re number is obtained, although the values still within the laminar regime threshold.

Table 2. Values of the Reynolds number (Re) for the different designs at different flow rates.

	Reynolds number (Re)				
	Flow rate (µL/min)				
3D Design	10	50	100	300	1000
TV1	0.335	1.674	3.348	10.044	33.481
TV2	0.167	0.833	1.667	5.000	16.667
SR1	0.333	1.667	3.333	10.000	33.333
SR2	0.167	0.833	1.667	5.000	16.667
CE1	0.952	4.762	9.524	28.571	95.238
CE2	0.952	4.762	9.524	28.571	95.238
CE3	0.333	1.667	3.333	10.000	33.333
CE4	0.167	0.833	1.667	5.000	16.667
VS1	2.381	11.905	23.810	71.429	238.095
VS2	2.381	11.905	23.810	71.429	238.095
VS3	1.667	8.333	16.667	50.000	166.667

5.1.2. Stokes number (Stk)

To fully evaluate our system, tracer particles were introduced in the aqueous solution, revealing not only the fluid flow but also to better understand the effect that chaotic cell units would have on the resulting mixing. First of all, it was necessary to determine the Stokes number to understand the potential motion tendency of the particle along the microfluidic system.

For the particle tracking test, the tracer had to be easy detect, non-reactive and present a behavior directly proportional to the fluid flow dynamic in order to follow the streamlines without changing its path, enabling a proper experimental validation results.

As explained in section 4.3.1, the particle used for the particle tracking test was UMDG001 COMPEL™ Fluorescent Magnetic COOH. The tracer had a particle density of ρ_p = 1200 kg/m3 particle diameter of d_p^2 = 3 µm. Equation (11) was employed for the numerical solutions of the Stk number. It should be noted that neither magnetic fields nor fluorescence microscope were used in these experiments, as the particles were just chosen for presenting a good dispersion in aqueous solution and a proper size range for the undergoing experimental studies.

The value of the Stokes number obtained for all the designs at different flow rates is below 1, indicating that particles have low inertia and will follow the fluid streamlines, meaning that the particle will be responsive to changes in flow, providing reliable results (See in Table 3).

For all microfluidic geometries and tested flow conditions, the resulting Stokes numbers were below one (Stk ≪ 1), indicating that the particle inertia is negligible. Consequently, the particles closely follow the pathlines of the streamline being sensitive to changes in flow, thereby enabling precise visualization and analysis of fluid pathlines.

Table 3. Values of the Stokes number (Stk) for the different designs at different flow rates.

	Stokes number (Stk)				
	Flow rate (µL/min)				
3D Design	10	50	100	300	1000
TV1	9.63E-09	4.82E-08	9.63E-08	2.89E-07	9.63E-07
TV2	1.20E-09	5.99E-09	1.20E-08	3.59E-08	1.20E-07
SR1	7.16E-09	3.58E-08	7.16E-08	2.15E-07	7.16E-07
SR2	1.59E-09	7.95E-09	1.59E-08	4.77E-08	1.59E-07
CE1	5.16E-08	2.58E-07	5.16E-07	1.55E-06	5.16E-06
CE2	5.16E-08	2.58E-07	5.16E-07	1.55E-06	5.16E-06
CE3	1.81E-08	9.03E-08	1.81E-07	5.42E-07	1.81E-06
CE4	2.26E-09	1.13E-08	2.26E-08	6.77E-08	2.26E-07
VS1	2.67E-06	1.34E-05	2.67E-05	8.01E-05	2.67E-04
VS2	2.67E-06	1.34E-05	2.67E-05	8.01E-05	2.67E-04
VS3	1.87E-06	9.35E-06	1.87E-05	5.61E-05	1.87E-04

5.1.3. Peclet Number (Pe)

To evaluate Peclet number, the molecular diffusion of the tracer was calculated. The equation used to obtain the molecular diffusion was the Stokes – Einstein equation (13). This equation characterizes the translational diffusion coefficient of the microspheres [32]:

$$D = \frac{k_B T}{6\pi\mu r} \qquad (13)$$

Where K_B is the Boltzmann constant (K_B = 1.38·10^{-23} J/K), T is the absolute temperature and r is the radius of the particle. Assuming values of temperature at T = 298 K, water viscosity of µ = 0.001 Pa·s and radius of r = 1.5·10^{-6} m, the resulting molecular diffusion of the tracers is D = 1.6·10^{-13} m^2/s. Subsequently, Pe was calculated with Equation (12).

The values obtained in Table 4. present values of Pe numbers above one (Pe ≫ 1), indicating that convection governs over molecular diffusion as the mass transport mechanism, providing us with a better understanding about the scalar quantities.

Table 4. Values of the Pe number (Pe) for the different designs at different flow rates.

	Peclet number (Pe)				
	Flow rate (µL/min)				
3D Design	10	50	100	300	1000
TV1	9.50E+07	4.75E+08	9.50E+08	2.85E+09	9.50E+09
TV2	4.72E+07	2.36E+08	4.72E+08	1.42E+09	4.72E+09
SR1	1.62E+08	8.09E+08	1.62E+09	4.85E+09	1.62E+10
SR2	8.09E+07	4.04E+08	8.09E+08	2.43E+09	8.09E+09
CE1	2.64E+08	1.32E+09	2.64E+09	7.91E+09	2.64E+10
CE2	2.64E+08	1.32E+09	2.64E+09	7.91E+09	2.64E+10
CE3	9.23E+07	4.61E+08	9.23E+08	2.77E+09	9.23E+09
CE4	4.61E+07	2.31E+08	4.61E+08	1.38E+09	4.61E+09
VS1	5.45E+07	2.73E+08	5.45E+08	1.64E+09	5.45E+09
VS2	5.45E+07	2.73E+08	5.45E+08	1.64E+09	5.45E+09
VS3	3.82E+07	1.91E+08	3.82E+08	1.15E+09	3.82E+09

5.2. CFD SIMULATION RESULTS OF THE MICROFLUIDIC DEVICES

The CFD Simulations were carried out by following the protocol explained in section 3. The geometry of the microfluidic was first designed by taking as inspiration, designs implemented in industrial macro-scale applications with the goal of intentionally forcing the maximum contact between the components possible. This could be achieved by implementing bifurcations along the channel, enhancing the collisions between the resulting streamlines. TV design is a macroscale passive valve in which, depending on the flow direction of the fluid along the channel, the fluid will go faster or slower due to the bifurcations of the geometry [33]. In parallel, SR design presents ring-shaped bifurcations along a straight microchannel, forcing the collision of the streamlines after their bifurcation.

As simulations were performed, new modifications were implemented to the microfluidic channel design. For each designs, different boundary conditions were applied and simulated. This modifications included height, width, length, the depth of the ridges or the mixing cells. The results obtained from the CFD simulations of TV and SR (see pathline displays in Appendix 2), indicated an absence of chaotic streamlines in any of the working flow rates established.

Taking care of the designs of the TV and SR, the geometry of the main channel in both designs remains only in a 2D plane, limiting the possibility of chaotic streamlines, as the fluid flow maintains a laminar profile. To potentially achieve these chaotic flows, CE design was designed. As reported by Strook et al. (2002) [22], in CE design the geometry consisted in a curved main channel with different ridges placed every two curves and, each of them, with a different angle. With this approach in CE2 at a working flow rate of 300 µL/min, we observed streamline patterns, most likely to the implementation of the ridges. Although we obtained a different and promising results from the CE design, the chaotic streamlines were not as overstated as desired.

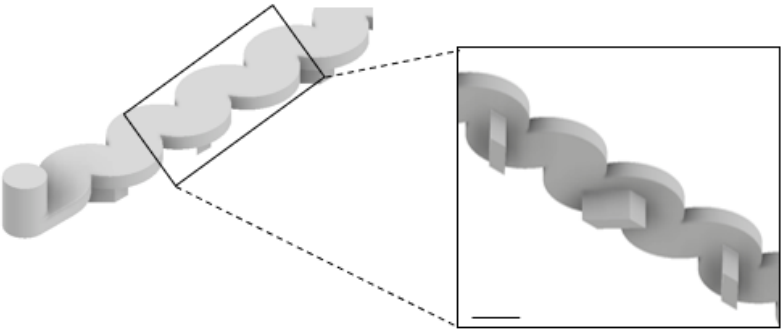

Figure 13. CE2 design and its corresponding bottom view. Scale bar at 0.5 mm

From the simulation results, we noted that the ratio of height and width had a significant effect on the flow behavior. Therefore, very high microchannels and ridges of low depth led to streamlines that negligees the presence of these ridges avoiding the possible change on the behavior of the flow maintaining its initial motion. In CE2 where the ratio between the width and height was smaller, the tendency of the flow was different from the other designs, flowing inside the ridges and then reincorporating again to the streamline. Having this effect in mind, VS microfluidic geometry was designed. The geometry consisted of a conventional serpentine implemented with inverted cones along the microchannels, which were referred to as chaotic mixing cells or mixing chambers. With this approach, the CFD simulation performances were successful, achieving chaotic flow in a controlled manner, as well as achieving spatial control by confining the potential mixing in the mixing cells. In Table 5 it is shown from which flow rate and which VS model these chaotic flows start to be visualized.

Table 5. Presence of Chaotic Flows in different working flow rates for VS design.

	Chaotic Mixing				
	Flow rate (µL/min)				
3D Design	10	50	100	300	1000
VS1	🔴	🔴	🔴	🟢	🟢
VS2	🔴	🔴	🔴	🟢	🟢
VS3	🔴	🔴	🟢	🟢	🟢

5.3. OPTIMIZATION OF THE LOC DEVICES

The first stage of the experimental procedure was focused on the optimization of the setup to work with the fabricated the microfluidic devices. During preliminary tests of streamline behavior via passive particle tracking, several problems were identified, such as bubbles and imperfections at channel junctions, despite following the protocol explained in section 4.4. To overcome this issue, the plasma bonding treatment between PDMS replica and glass substrate, was done on the very same date of the experimental tests. After the plasma bonding the microfluidic devices were placed on a heating plate at 125 ºC for 2 h and then cooled to room temperature for 15 min. By following this (i) plasma bonding approach, as well as (ii) flushing isopropanol the first time a microfluidic device used, followed with three sequential flush with water to remove any traces of isopropanol, and (iii) the droplet-to-droplet tubing connections explained in section 4.4, we managed to maintain the hydrophobic properties of the LoC device and avoid bubbles during the experiments.

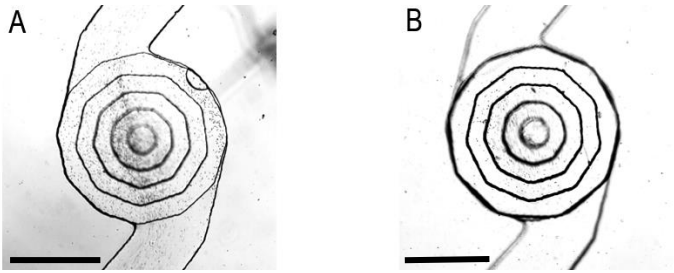

Figure 14. Bright Field images of the third mixing cell of VS3 design. A) Tracking Particles Test. B) Particle Tracking Test optimized. Scale bars 0.5 mm

5.4. EXPERIMENTAL RESULTS

5.3.1. Microparticles used as tracers

Due to time constraints, we only managed to capture the particle motion on one of the mixing chambers of VS designs. In addition, the range of motion was limited as the lens could not focus on the full mixing chamber and only allowing the visualization of one layer of the mixing cell. All tat different flow rates are found in Annex 3.

For the three variations of the VS designs, chaotic flows or vortices started to appear at a working flow rate of 300 µL/min (see in Figure 15).

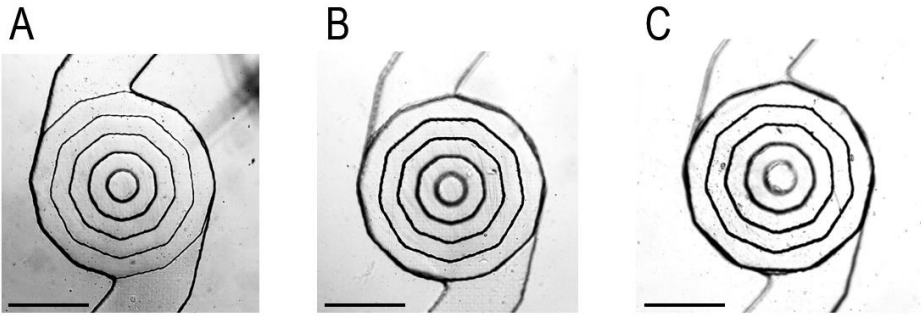

Figure 14. Bright Field images of the third mixing cell of VS3 design at 300 µL/min . A) VS1, B) VS2, C) VS3. As it can be observed, vortex is only facilitated by VS3. Scale bars 0.5 mm.

5.3.2. Dye color mixing test

In order to evaluate the mixing behavior in both Y-Shaped channels and VS channel, we used two different colored dyes, blue and red. It can be observed that while in the Y-shaped channel just laminar flow regime takes place, in the VD channel efficient mixing is occurring in the chaotic mixing cells working at 300 µL/min, as seen in the microparticles tracking experiments. Experiments at different flow rates with both designs are included in Annex 3.

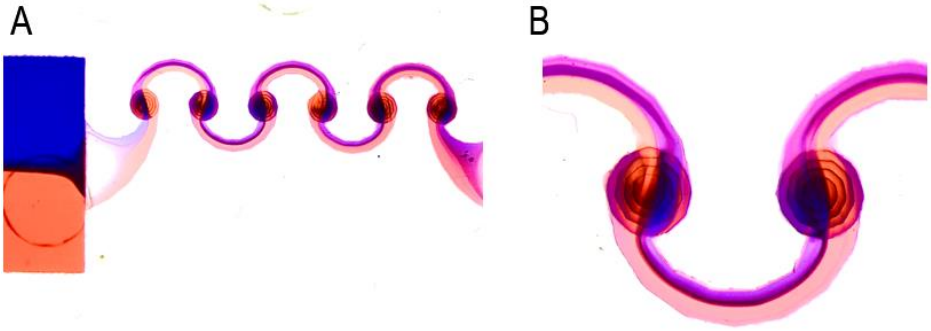

Figure 15. Dye color test. Flow rate at 300 300 µL/min. A) Y-Shaped channel with VS3 implemented. B) Closer top view of chaotic mixing cells 2 and 3.

5.3.3. Electrochemical validation

After simulating and experimentally evaluating the mixing efficiency of the different designs studied in section 5.3.1 and 5.3.2, we determined that the best microfluidic device to be implemented in the electrochemical studies was VS3. The electrochemical experiments were performed by Irene Vilà i Cibantos in her TFG, optimizing the best conditions for the Prussian Blue detection by using screen-printed electrodes (SPCEs) integrated in LoC devices. One of the main challenges in such electrochemical studies is the mass transport of the analyte of interest (in our case PB) to the working electrode to increase its sensitivity. By integrating such enhanced mixing was taking place just before the SPCEs, increasing mixing reaction efficiency of the Sol A (10 mM $Fe(NO_3)_3 \cdot 9H_2O$, 10 mM $K_3[Fe(CN)_6]$, 0.1 M KCl, Buffer pH 5) and Sol B (L-Ascorbic Acid in aqueous solution).The corresponding electrode characterization and applied potential during the electrochemical tests are described in the Irene Vilà i Cibantos TFG (*Integration of miniaturized sensors in lab on a chip devices for enhanced mass transport efficiency* in Chemistry supervised by Dr. Maria Guix and Dr Julio Batos Arrieta). Once the electrochemical system was optimized, the experimental test with the Vortex Street design were performed, demonstrating that as flow rate increases (same flow rate applied in each channel), the resulting current becomes more negative, as it contains higher iron (III) concentration. In Figure 16, we can observe that when performing the experiments with both Solution A and Solution B (yellow chronoamperometry in Fig. 16) and increasing the flow rates, the electrochemical signal comes closer to the signal of an already-mixed PB solution (solution used as reference, blue chronoamperometry in Fig. 16). Indeed, we observed an appreciable improvement already in 200 µl/min, although our simulations

predicted such optimal mixing at 300 µl/min. At 1000 µl/min the current becomes unstable due to leakage associated to the overpressure applied in the high flow rate. However, we tested it to compare it with the corresponding simulations. Therefore, the experimental results present a good correlation to the simulations performed for the Vortex Street, even showing an efficient mixing before the expected flow rate, at 200 µl/min.

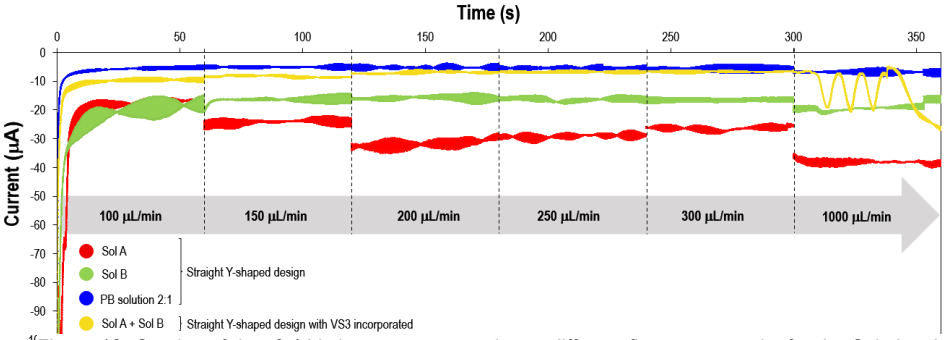

Figure 16. Overlay of the -0.4 V chronoamperometries at different flow rates results for the Solution A, Solution B (50 mM ascorbic acid solution), already generated Prussian Blue solution 2:1 (Fe3+:AA, used as reference), and the final Sol A+ Sol B mixture (adapted from Irene Vilà Cibantos TFG).

6. CONCLUSIONS

In this TFG we have,

- Designed and fabricated microfluidic channels to obtain controlled spatial mixing under fluid domains governed by laminar regimes.

- Simulated the different microfluidic designs by using Autodesk Inventor and carrying out CFD simulations with ANSYS Workbench R2 to evaluate the fluid flow performances along different geometries, providing us a reliable and accurate results to decide the best microfluidic chips to use, optimizing time and resources.

- Fabricate the best chip by combining 3D printing technologies and microfabrication techniques (PMDS molding), allowing to obtain in a very precise complex geometry, offering a wide range of possibilities and applications for any scientific field.

- Demonstrated the local mixing capacity of the chaotic mixing cells included in the microfluidic chip by using both visualization experiments (e.g., tracking tracers in chip, mixing of colored dyes), and electrochemical studies.

- Environmental and economic potential: the methods proposed in this project show promise in microscale industrial technology, enabling potential passive micromixers which mixing is controlled. With this said, the industrial applications at a microscale can provide synthetic results reducing the resource consumption of substrates.

- Simulated the different microfluidic designs by using Autodesk Inventor and carrying out CFD simulations with ANSYS Workbench R2 to evaluate the fluid flow performances along different geometries, providing us a reliable and accurate results

to decide the best microfluidic chips to use, optimizing time and resources. The best design, taken for the experimental studies, was the VS because of the working flow rates that provide us chaotic mixing.

7. FUTURE WORKS

Further research may be conducted from multiple perspectives, such as comprehensive experimental validation, modification of boundary conditions, and development of new geometrical configurations derived from the existing designs to optimize performance metrics.

Moreover, this research presents a general approach to microscale mixing enhancement, offering improved performance across diverse applications, ranging from materials synthesis to inducing on-demand chirality in certain compounds to the enhancement of analytical sensitivity in several analytical techniques. Therefore, subsequent investigations may integrate this framework into domain-specific contexts and explore complementary microfluidic strategies that remain underexplored.

REFERENCES AND NOTES

[1] N. Contreras-Pereda *et al.*, "Synthesis of 2D Porous Crystalline Materials in Simulated Microgravity," *Advanced Materials*, vol. 33, no. 30, Jul. 2021, doi: 10.1002/adma.202101777.

[2] J. Castillo-Leon and W. E. Svendsen, *Lab-on-a-Chip Devices and Micro-Total Analysis Systems*, 1st ed. Cham: Springer International Publishing, 2015. doi: 10.1007/978-3-319-08687-3.

[3] K. F. Lei, "Introduction: The Origin, Current Status, and Future of Microfluidics," in *Microfluidics: Fundamental, Devices and Applications*, Wiley, 2018, pp. 1–18. doi: 10.1002/9783527800643.ch1.

[4] G. M. Whitesides, "The origins and the future of microfluidics," *Nature*, vol. 442, no. 7101, pp. 368–373, Jul. 2006, doi: 10.1038/nature05058.

[5] M. Gonidec and J. Puigmartí-Luis, "Continuous- versus Segmented-Flow Microfluidic Synthesis in Materials Science," *Crystals (Basel)*, vol. 9, no. 1, p. 12, Dec. 2018, doi: 10.3390/cryst9010012.

[6] P. N. Nge, C. I. Rogers, and A. T. Woolley, "Advances in Microfluidic Materials, Functions, Integration, and Applications," *Chem Rev*, vol. 113, no. 4, pp. 2550–2583, Apr. 2013, doi: 10.1021/cr300337x.

[7] D. C. Duffy, J. C. McDonald, O. J. A. Schueller, and G. M. Whitesides, "Rapid Prototyping of Microfluidic Systems in Poly(dimethylsiloxane)," *Anal Chem*, vol. 70, no. 23, pp. 4974–4984, Dec. 1998, doi: 10.1021/ac980656z.

[8] S. Kim, J. Kim, Y.-H. Joung, J. Choi, and C. Koo, "Bonding Strength of a Glass Microfluidic Device Fabricated by Femtosecond Laser Micromachining and Direct Welding," *Micromachines (Basel)*, vol. 9, no. 12, p. 639, Dec. 2018, doi: 10.3390/mi9120639.

[9] S. K. Sia and G. M. Whitesides, "Microfluidic devices fabricated in Poly(dimethylsiloxane) for biological studies," *Electrophoresis*, vol. 24, no. 21, pp. 3563–3576, Nov. 2003, doi: 10.1002/elps.200305584.

[10] S. A. Jaywant and K. M. Arif, "A Comprehensive Review of Microfluidic Water Quality Monitoring Sensors," *Sensors*, vol. 19, no. 21, p. 4781, Nov. 2019, doi: 10.3390/s19214781.

[11] T. O. Hara and B. Singh, "Electrochemical Biosensors for Detection of Pesticides and Heavy Metal Toxicants in Water: Recent Trends and Progress," *ACS ES&T Water*, vol. 1, no. 3, pp. 462–478, Mar. 2021, doi: 10.1021/acsestwater.0c00125.

[12] L. Wang, W. Qi, Y. Liu, D. Essien, Q. Zhang, and J. Lin, "Recent Advances on Bioaerosol Collection and Detection in Microfluidic Chips," *Anal Chem*, vol. 93, no. 26, pp. 9013–9022, Jul. 2021, doi: 10.1021/acs.analchem.1c00908.

[13] P. Tabeling, “Introduction,” in *Introduction to Microfluidics*, Oxford University PressOxford, 2023, pp. 1–47. doi: 10.1093/oso/9780192845306.003.0001.

[14] B. Xu, Y. Zhang, S. Wei, H. Ding, and H. Sun, “On-Chip Catalytic Microreactors for Modern Catalysis Research,” *ChemCatChem*, vol. 5, no. 8, pp. 2091–2099, Aug. 2013, doi: 10.1002/cctc.201200863.

[15] K. F. Jensen, “Microreaction engineering — is small better?,” *Chem Eng Sci*, vol. 56, no. 2, pp. 293–303, Jan. 2001, doi: 10.1016/S0009-2509(00)00230-X.

[16] A. Isozaki *et al.*, “AI on a chip,” *Lab Chip*, vol. 20, no. 17, pp. 3074–3090, 2020, doi: 10.1039/D0LC00521E.

[17] K. F. Jensen, “Flow chemistry—Microreaction technology comes of age,” *AIChE Journal*, vol. 63, no. 3, pp. 858–869, Mar. 2017, doi: 10.1002/aic.15642.

[18] H. Jigar Panchal, N. J. Kent, A. J. S. Knox, and L. F. Harris, “Microfluidics in Haemostasis: A Review,” *Molecules*, vol. 25, no. 4, p. 833, Feb. 2020, doi: 10.3390/molecules25040833.

[19] D. Curcó, “Apunts Fenòmens de Transport,” Universitat de Barcelona, Barcelona, 2024.

[20] Y. Song, X. Zhao, Q. Tian, and H. Liang, “Fundamental Concepts and Physics in Microfluidics,” in *Microfluidics: Fundamental, Devices and Applications*, Wiley, 2018, pp. 19–111. doi: 10.1002/9783527800643.ch2.

[21] P. Tabeling, “Hydrodynamics of microfluidics 1: channels,” in *Introduction to Microfluidics*, Oxford University PressOxford, 2023, pp. 103–161. doi: 10.1093/oso/9780192845306.003.0003.

[22] A. D. Stroock, S. K. W. Dertinger, A. Ajdari, I. Mezić, H. A. Stone, and G. M. Whitesides, “Chaotic Mixer for Microchannels,” *Science (1979)*, vol. 295, no. 5555, pp. 647–651, Jan. 2002, doi: 10.1126/science.1066238.

[23] H. K. Versteeg and W. Malalasekera, *An Introduction to Computational Fluid Dynamics: The Finite Volume Method*, 2nd ed. 2007.

[24] N. Padoin, T. Matiazzo, H. G. Riella, and C. Soares, “A perspective on the past, the present, and the future of computational fluid dynamics (CFD) in flow chemistry,” *J Flow Chem*, vol. 14, no. 1, pp. 239–256, Mar. 2024, doi: 10.1007/s41981-024-00313-4.

[25] A. Lintermann, “Computational Meshing for CFD Simulations,” 2021, ch. Chapter 6, pp. 85–115. doi: 10.1007/978-981-15-6716-2_6.

[26] J. Aubin, D. F. Fletcher, and C. Xuereb, “Design of micromixers using CFD modelling,” *Chem Eng Sci*, vol. 60, no. 8–9, pp. 2503–2516, Apr. 2005, doi: 10.1016/j.ces.2004.11.043.

[27] J. Blazek, “Consistency, Accuracy, and Stability,” in *Computational Fluid Dynamics: Principles and Applications*, Elsevier, 2015, pp. 337–356. doi: 10.1016/B978-0-08-099995-1.00010-5.

[28] I. Sadrehaghighi, *Mesh Generation in CFD*. 2020.

[29] Y. Xia *et al.*, “Covalent transfer of chemical gradients onto a graphenic surface with 2D and 3D control,” *Nat Commun*, vol. 13, no. 1, p. 7006, Nov. 2022, doi: 10.1038/s41467-022-34684-w.

[30] A. Borók, K. Laboda, and A. Bonyár, “PDMS Bonding Technologies for Microfluidic Applications: A Review,” *Biosensors (Basel)*, vol. 11, no. 8, p. 292, Aug. 2021, doi: 10.3390/bios11080292.

[31] S. Sevim *et al.*, "Chirality transfer from a 3D macro shape to the molecular level by controlling asymmetric secondary flows," *Nat Commun*, vol. 13, no. 1, p. 1766, Apr. 2022, doi: 10.1038/s41467-022-29425-y.

[32] A. Baer *et al.*, "The Stokes–Einstein–Sutherland Equation at the Nanoscale Revisited," *Small*, vol. 20, no. 6, Feb. 2024, doi: 10.1002/smll.202304670.

[33] K. Vaferi *et al.*, "Modeling and Optimization of Hydraulic and Thermal Performance of a Tesla Valve Using a Numerical Method and Artificial Neural Network," *Entropy*, vol. 25, no. 7, p. 967, Jun. 2023, doi: 10.3390/e25070967.

[34] H. R. Sahoo, J. G. Kralj, and K. F. Jensen, "Multistep Continuous-Flow Microchemical Synthesis Involving Multiple Reactions and Separations," *Angewandte Chemie International Edition*, vol. 46, no. 30, pp. 5704–5708, Jul. 2007, doi: 10.1002/anie.200701434.

ACRONYMS AND SYMBOLS

LoC: Lab-on-a-chip

μTAS: micro-total analysis system

MRT: Microreaction Technology

σ: shear stress

γ: shear rate

Re: Reynolds number

Stk: Stokes number

Pe: Peclet number

PDMS: polydimethylsiloxane

SLA: stereolithography

CFD: computational fluid dynamics

Sol A: Solution A

Sol B: Solution B

PB: Prussian Blue

TV: Tesla Valve

SR: Straight with Rings

CE: Curves and Eddies

VS: Vortex Street

SPCEs: screen-printed electrodes

APPENDICES

APPENDIX 1: DIMENSIONS OF THE MICROFLUIDIC DEVICES

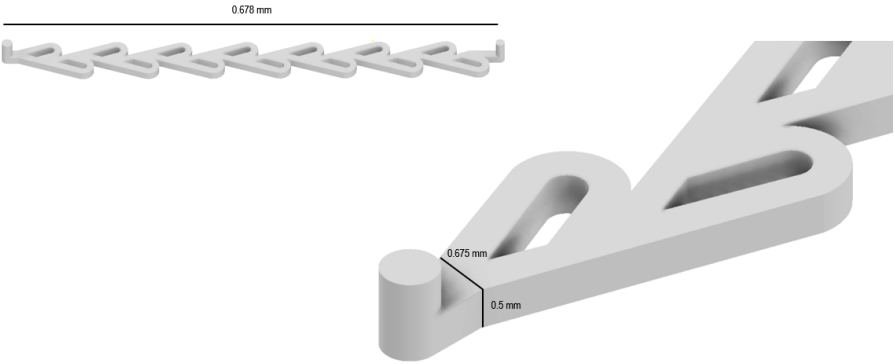

Figure 17. TV1 design.

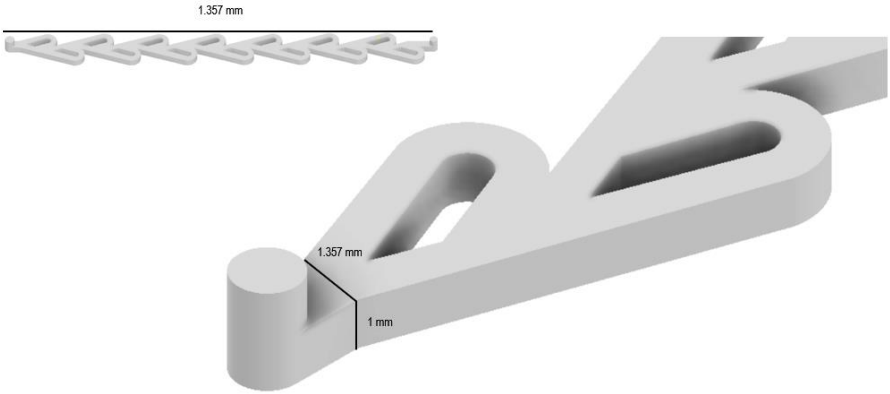

Figure 18. TV2 design.

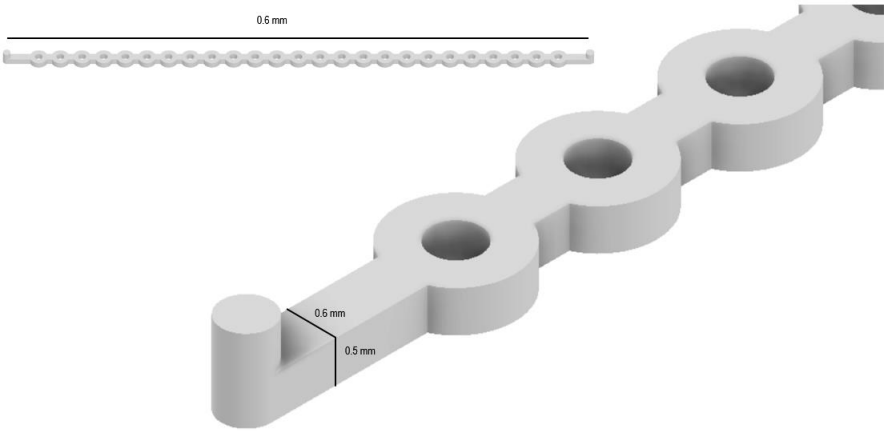

Figure 19. SR1 design.

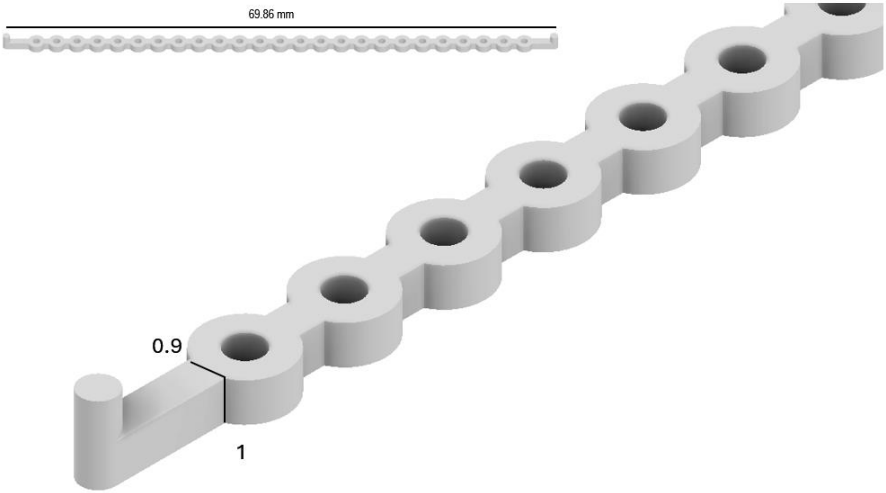

Figure 20. SR2 design.

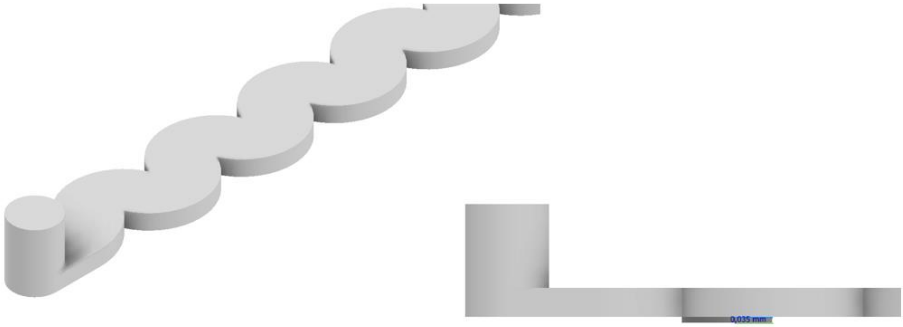

Figure 21. CE1 design.

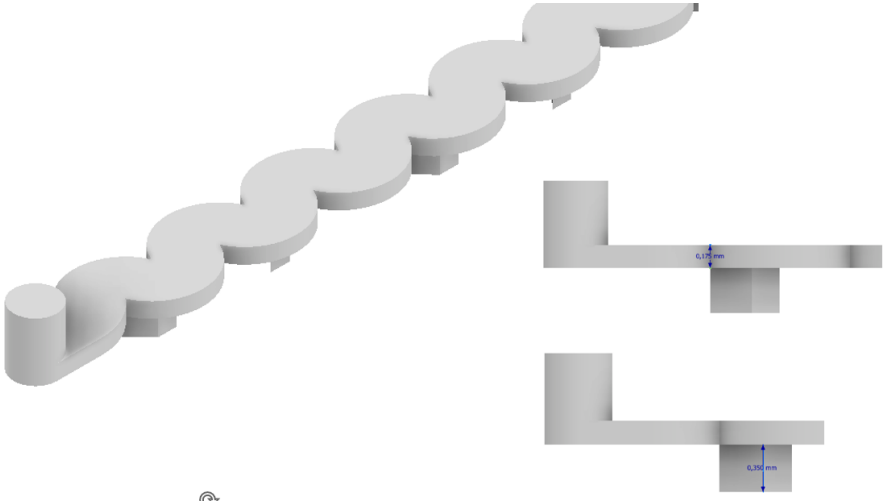

Figure 21. CE2 design.

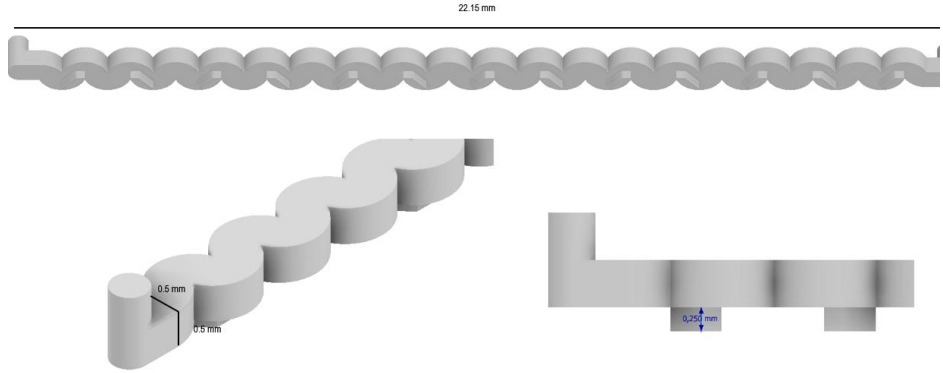

Figure 21. CE3 design.

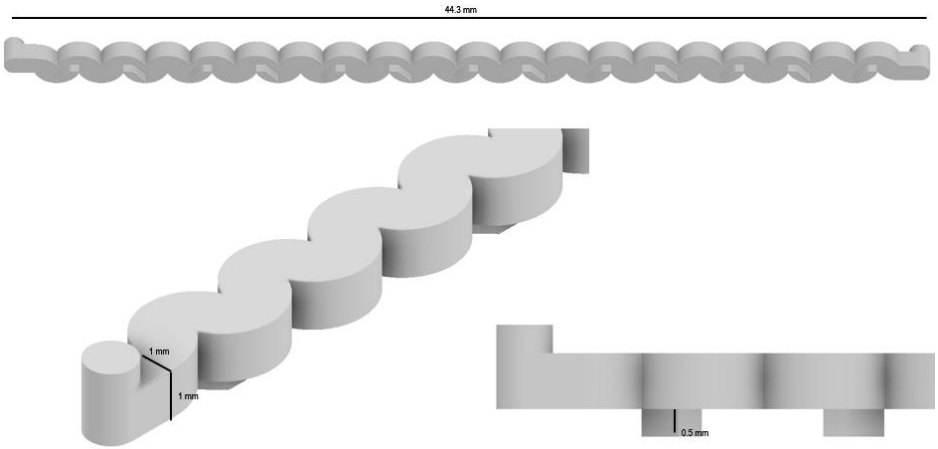

Figure 22. CE4 design.

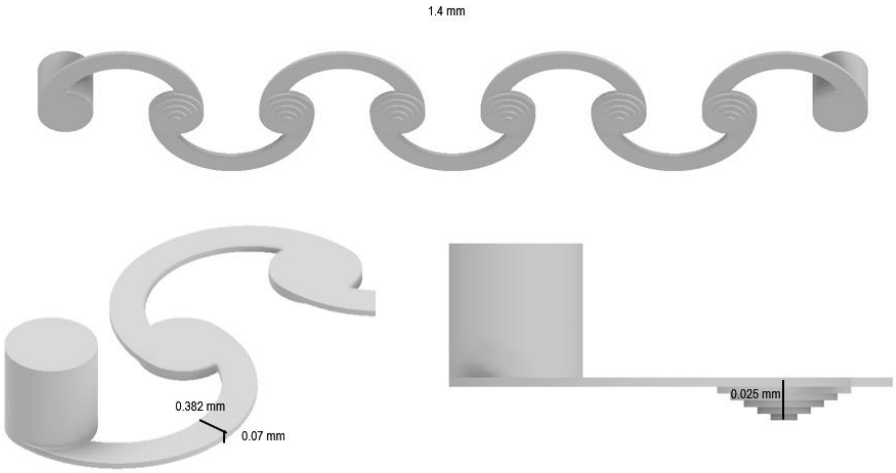

Figure 23. VS1 design.

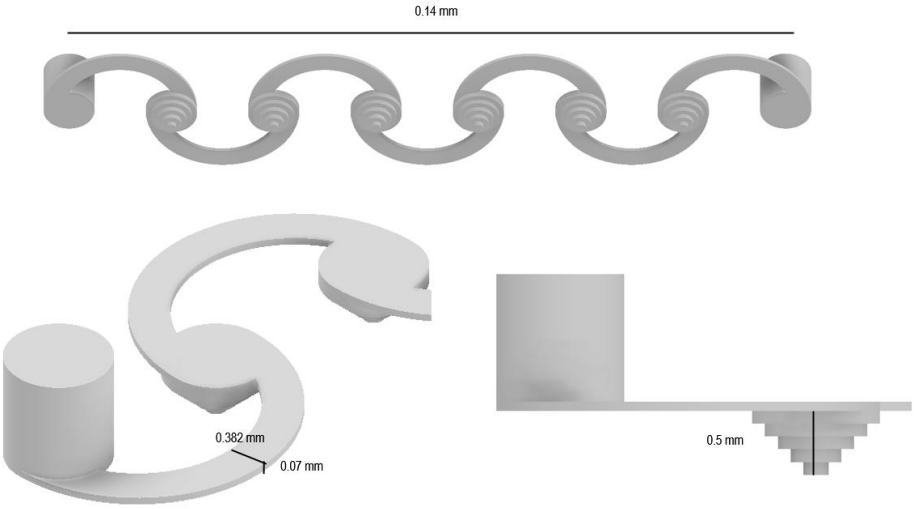

Figure 24. VS2 design.

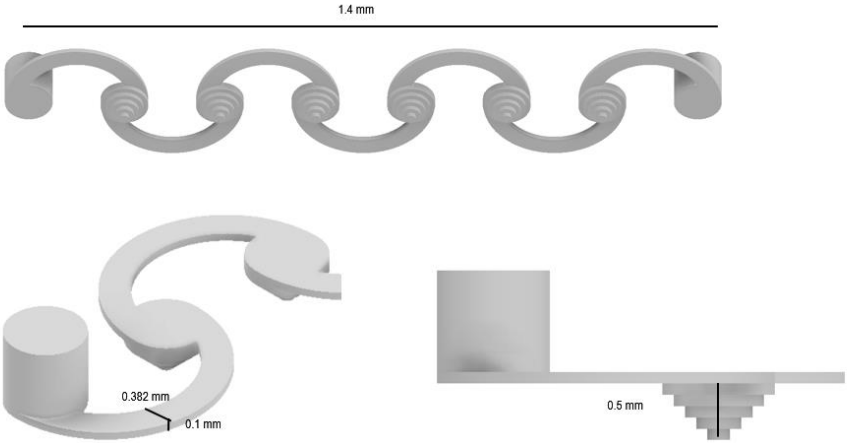

Figure 25. VS3 design.

APPENDIX 2: PATHLINE DISPLAY OF THE CFD SIMULATIONS

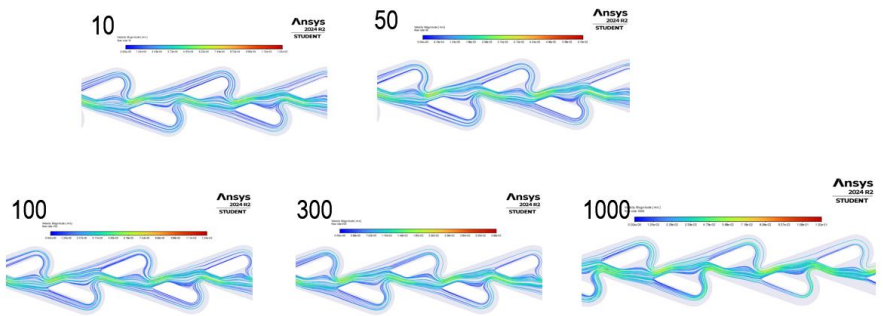

Figure 25. TV1 simulation.

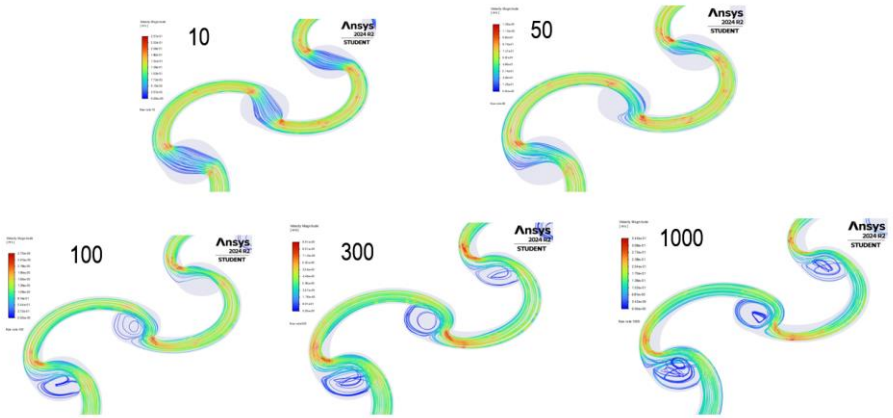

Figure 26. TV1 simulation.

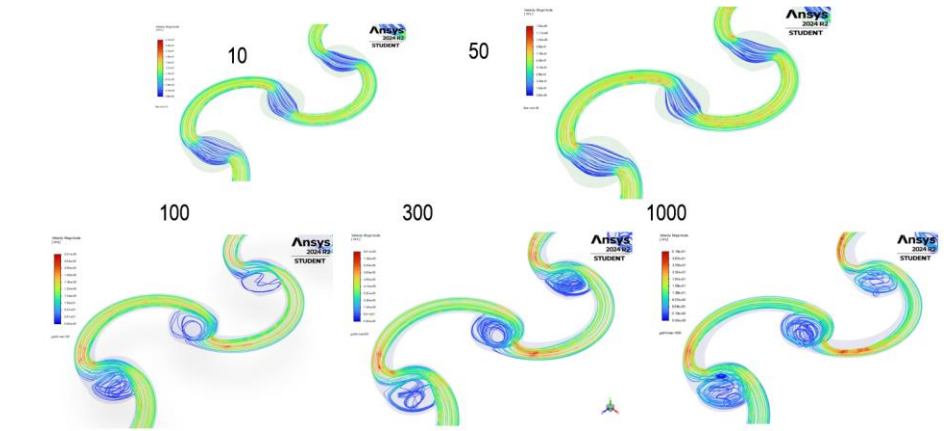

Figure 27. TV2 simulation.

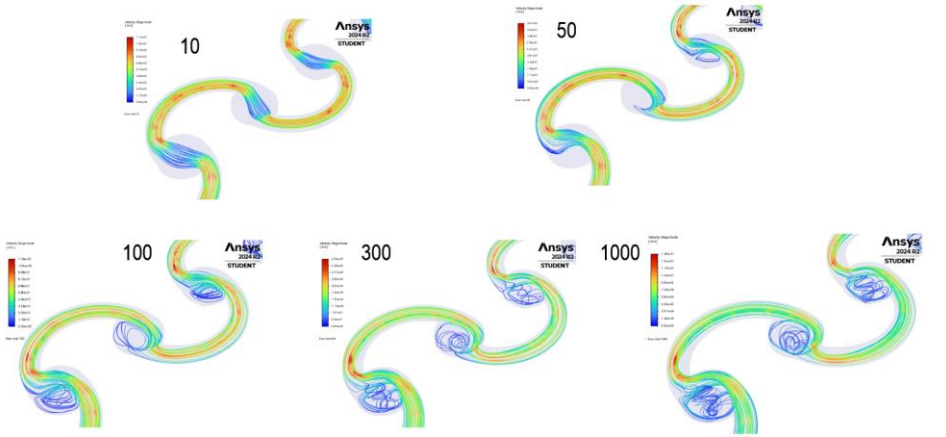

Figure 28. TV2 simulation.

APPENDIX 3: EXPERIMENTAL VIDEOS

Microparticle Tracking videos: OneDrive

Dye Color Mixing Test videos: OneDrive